Gap Junction Channels and Hemichannels

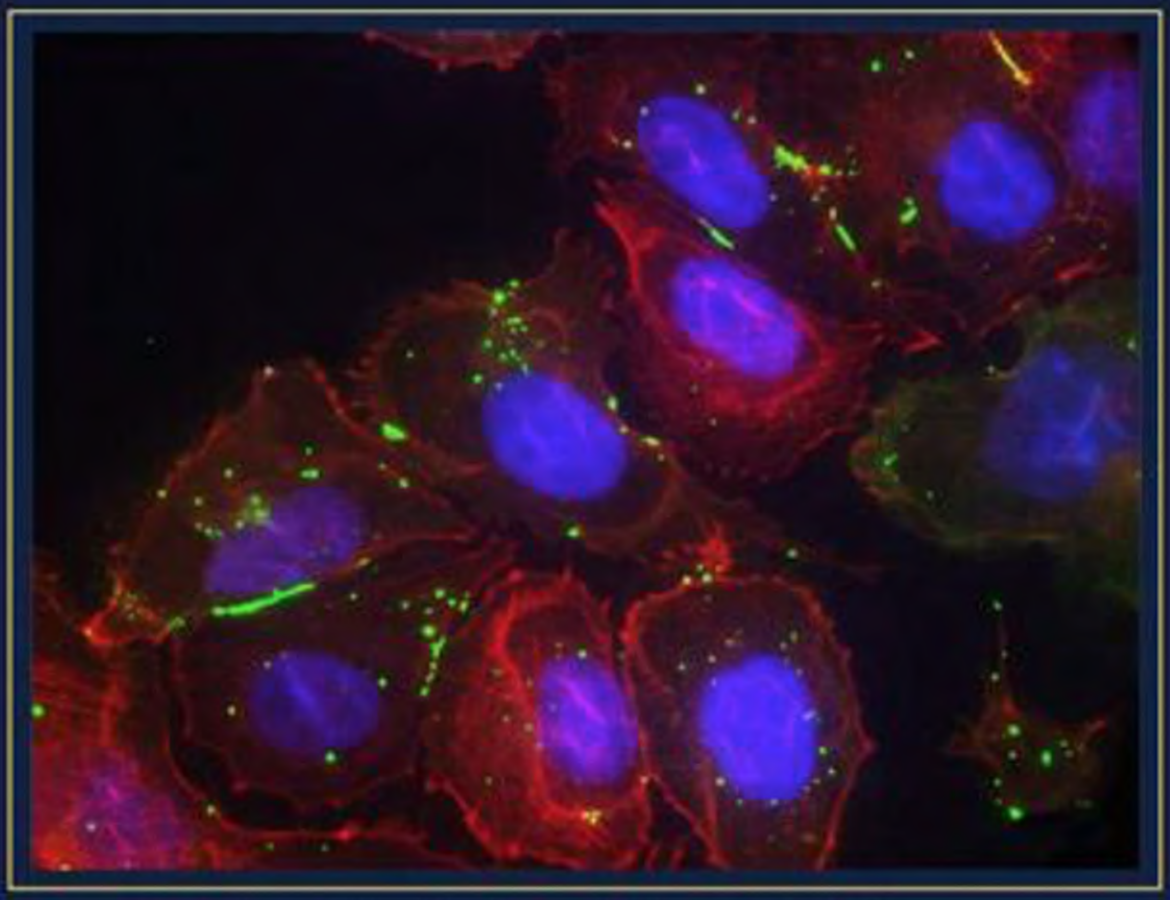

Edited by Donglin Bai and Juan C. Sáez

METHODS IN SIGNAL TRANSDUCTION SERIES

CRC Press
Taylor & Francis Group

2 Imaging Gap Junctions in Living Cells

Matthias M. Falk, Charles G. Fisher, Rachael M. Kells Andrews, and Tia J. Kowal

CONTENTS

2.1 INTRODUCTION

Research over the past years has shown that gap junctions, comprised of connexins, are highly dynamic structures. Connexins are synthesized, oligomerized into connexons, trafficked to the plasma membrane, docked into double-membrane spanning gap junction channels, assembled into gap junction plaques, internalized, and degraded. This dynamic nature apparently ensures proper gap junction function by regulating the level of direct cell-to-cell communication and of physical cell–cell adhesion. Gap junction dynamics correlates with the short half-life of connexins that has been determined to range from 1–5 hours in vivo and in situ (Berthoud et al. 2004). The dynamics of protein structures such as gap junction channels are best studied and demonstrated in live cells. To investigate the individual steps of the life cycle of connexins and gap junctions over time, the time-lapse imaging of fluorescently tagged connexins appears to be the most suitable method, as it provides spatiotemporal resolution in real time. Imaging fixed cells with either fluorescently tagged connexins or untagged connexins stained with a fluorophore is useful for colocalization studies of connexins with associated proteins. Additionally, it can offer hints at the dynamics of the gap junctions when fixing and analyzing multiple dishes at successive time points. However, fixed cells cannot offer real-time analysis of the dynamics of the gap junctions. Biochemical studies of gap junctions, which usually involve western blotting, can give a broad picture of the total connexin population in cells, but cannot offer information on the dynamics of individual gap junction plaques. Hence, a combination of approaches including biochemical and imaging analyses appears most desirable and is likely to produce the most convincing results. In the following sections, we provide an overview of live-cell imaging techniques as

they have been applied over the past two decades in the authors' laboratory to investigate the biosynthesis, the structure, and the function of gap junctions. We briefly discuss microscope requirements, fluorescent probes, and imaging systems. Then we discuss how to image specific stages of the gap junction life cycle such as trafficking, endocytosis, and degradation. Next, we describe how to make observations of the gap junction plaque structure and dynamics, the colocalization of gap junctions with their binding partners, and how to conduct quantitative fluorescence analysis of these observations. We then explain the techniques to allow for the imaging of gap junctions in living cells for several days without significant detrimental side effects. Finally, we point out pitfalls and typical mistakes that can occur when conducting live-cell observations on gap junctions and give hints and tips on how to avoid them.

2.2 LIVE-CELL MICROSCOPE EQUIPMENT

Imaging living cells over time requires forethought, planning, and special equipment to maintain the cells at physiological conditions. Time-lapse imaging of gap junctions can be accomplished either through consistent manual imaging by the operator or with an automated live-cell video microscope. In general, an automated system is preferable to a manual system because most time-lapse sessions can last for hours and require the user to open and close illumination shutters, rotate filters, correct focal drift, and potentially track several positions all while maintaining identical time intervals for the entire recording session. Another major advantage of automated systems is that the cells are exposed to excitation light only during exposures, which reduces negative, light-induced effects (see Section 2.2.6). Of course, automation comes with an extra price tag, easily selling for tens of thousands of dollars.

2.2.1 Cell Culture Conditions

Imaging metabolically driven processes in live mammalian cells requires maintaining normal physiological conditions over time. These include maintaining the cells at 37°C, 100% humidity, a pH of about 7.5, and a steady unlimited nutrient supply. Conditions such as these are normally provided in a standard laboratory cell culture incubator. However, outside of the incubator conditions can rapidly change due to lower ambient room temperature and lower CO_2 concentration of air. Indeed, most dynamic processes in mammalian cells come to a halt at ≤20°C (Saraste et al. 1986; Fuller et al. 1985; Saraste and Kuismanen 1984; Matlin and Simons 1983; Rotundo and Fambrough 1980), so at the very least, a temperature equivocal to body temperature needs to be maintained. Moreover, the pH of the culture medium, which is normally adjusted to pH 7.5 at 5% CO_2 atmosphere, can rise within minutes above pH 8, creating conditions that are clearly not physiologically ideal and can adversely affect cellular processes, including dynamics. If live-cell image recordings are designed to last only a few minutes, the issues mentioned earlier may not pose severe problems since the temperature can be maintained by placing a small heater or a hair dryer within close range of the microscope stage. The culture medium may also be amended with 4-(2-hydroxyethyl)-1-piperazineethanesulfonic (HEPES) acid buffer (10–25 mM), which maintains the physiological pH of the medium when outside

of the incubator. Any culture medium that is normally supplemented with phenol red as a pH indicator typically generates background fluorescence that is especially pronounced in the red fluorescence channel and may need to be replaced by a culture medium without a pH indicator (commercially available for standard medium formulations). Finally, oxygen free radicals, which are toxic to cells, are typically generated by the intense illumination energy in the culture medium (occurring on the microscope stage over time) and may need to be neutralized by the addition of OxyFluor™ (Oxyrase, Inc.) to the culture medium.

2.2.2 Microscope Setups

Live-cell imaging is typically performed on inverted microscopes, meaning the objectives are mounted below the microscope stage (Figure 2.1). This arrangement provides the most convenient setup, as it allows for the imaging of cells attached to

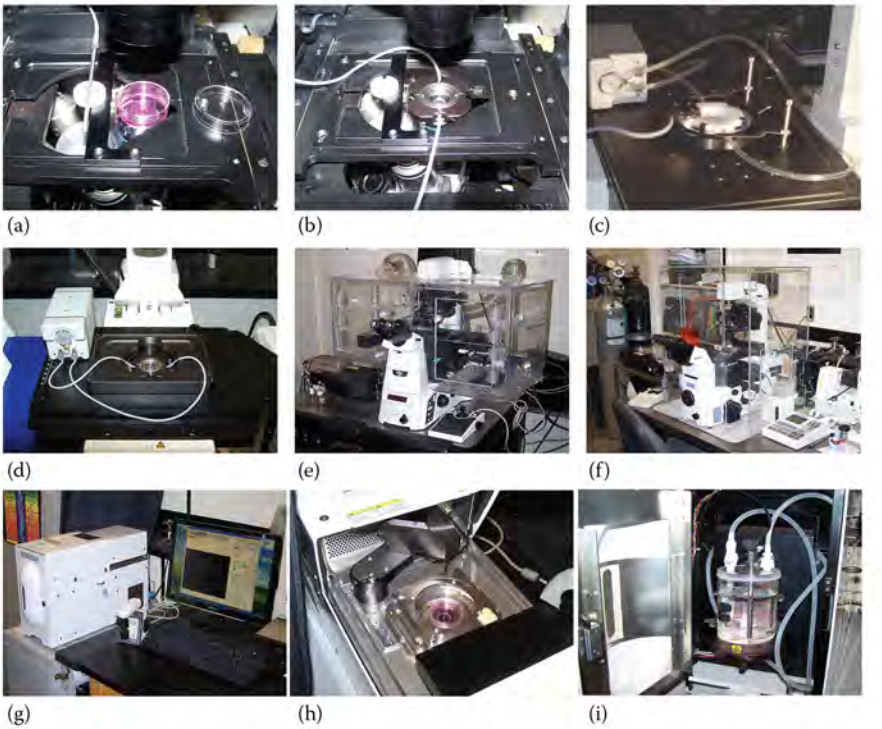

FIGURE 2.1 (See color insert.) Live-cell microscope equipment. Live cell chambers: (a) MatTek glass bottom dish, (b) POCmini, and (c) Focht Chamber System 2. (c, d) Peristaltic pumps used to circulate or exchange medium over time. Environmental incubators (e) partially or (f) entirely encasing microscopes. (g) Nikon's BioStation, a combined microscope/cell culture incubator, featuring (h) a temperature- and 5% CO_2-controlled imaging cell chamber, and (i) a gas bubbler to maintain 100% atmosphere humidity.

the bottom surface of a dish placed on the stage while keeping the cells immersed in the medium. However, conventional upright microscope systems can also be used for live-cell imaging if they are equipped with special commercially available dip-in objectives. The front lens on these objectives is specially sealed so that the tip can be submersed in the culture medium without damaging it due to corrosion. These objectives are water-immersion objectives that offer an intermediate quality (typical NA*: 0.8–1.2) to air (typical NA: ≤0.75) and oil immersion objectives (typical NA: ~1.4) (note that the NA of an objective directly dictates image resolution). For example, we have used 40× and 60× Nikon Fluor dip-in water-immersion objectives on an upright Nikon Eclipse E800 fluorescence microscope with satisfactory results.

2.2.3 Live-Cell Chambers

Standard cell/tissue culture (TC) polystyrene plastic dishes are not suitable for high-quality oil immersion objectives, as TC plastic is of poor optical quality compared to glass and is too thick to focus on cells in the dish. Specially designed cell culture dishes in which a portion of the bottom is replaced with a high-quality, 0.17 mm thick borosilicate glass coverslip that is coated with extracellular matrix proteins for cell adhesion (collagen, fibronectin, etc.) are commercially available (MatTek Corporation as well as other manufacturers) and are a convenient solution for many live-cell applications (Figure 2.1a). For longer time-lapse recordings, specially designed live-cell chambers such as the POCmini-2 (POC Cell Cultivation Systems, PeCon GmbH) and the Focht Chamber System 2 (FCS2®; Bioptechs) are commercially available (Figure 2.1b and c) and offer better control of environmental conditions, including medium exchange either by gravity or a peristaltic pump (Figure 2.1b through d).

2.2.4 Environmental Incubators

For longer time-lapse recordings that require maintaining 37°C for hours, the construction of environmentally controlled incubators that encase the microscope either partially or entirely is necessary (Figure 2.1e and f). These incubators not only keep the cells alive and metabolically active but also help with preventing focal drift (the gradual tendency of specimens to move out of focus over time), an issue that especially occurs when different parts of the microscope are maintained at different temperatures (ambient vs. 37°C). Of course, environmental incubators reduce the access to the working parts of the microscope; thus, multiple doors on all sides are desirable to ensure adequate access (see Figure 2.1e and f).

* NA = numerical aperture. The numerical aperture of a microscope objective is a measure of its ability to gather light and resolve specimen details. It is defined by $NA = n\sin\alpha$ (n represents the refractive index of the medium between the objective front lens and the specimen, and α is the one-half angular aperture of the objective).

2.2.5 Combined Microscope/Cell Culture Incubators

More recently, live-cell microscope systems that combine a cell culture incubator, a fluorescent microscope, and an air-cooled charge-coupled device (CCD) camera all in one convenient unit, such as Nikon's BioStation IM-Q (Figure 2.1g), have become commercially available at an affordable price. They optimize the environmental conditions and hence eliminate many of the detrimental issues that are prohibitory to extended live-cell recordings. These systems contain a heated live-cell chamber (Figure 2.1h) and are connected to a CO_2 tank. The consistency of the atmosphere is maintained by a gas mixer, which maintains 5% CO_2. The gas mixture is bubbled through a concealed water-filled jar (Figure 2.1i) before being pumped into the chamber, thus maintaining 100% humidity to prevent unintentional evaporation and concentration of the culture medium. These systems typically allow live-cell recordings for multiple days (with an image acquired every minute) even with short wavelength (blue light) illumination as shown for gap junctions in Figure 2.2a and b. The image resolution/quality is not typically as high as with high-end microscope systems described earlier. This is because the imaging is performed using lower numerical aperture, long-distance 20× and 40× objectives that can also be used at 10×, 20×, ×40, and ×80, depending on the configuration, by swinging additional collector lenses into the light path. However, as evident from image sequences shown in Figure 2.2a and b, the imaging quality is clearly sufficient to resolve the dynamics of the gap junctions in living cells, allowing one to follow their entire life cycle (from plaque assembly to degradation) over time. Two fluorescent wavelengths can be chosen and recorded in addition to phase contrast white light illumination. Additionally, multiple points of interest in the dish can be programmed in sequence, allowing for the simultaneous imaging of several locations (gap junctions) over time. As video microscopes are typically used for longer durations, it is critical to ensure that the microscope and the live-cell chamber function properly to maintain a favorable environment or else the cells will likely die during imaging, or irrelevant recordings of cells may be generated that do not reflect physiological conditions.

2.2.6 Potentially Toxic Effects of Excitation Light

A general issue associated with live cell imaging is phototoxicity, which is especially pronounced if high-energy short wavelength light (ultraviolet [UV], blue) is used for excitation (as is needed for cyan fluorescent protein [CFP] and green fluorescent protein [GFP]-excitation, see Section 2.4.2). Extensive illumination with bright light (either continuous or administered in repeated pulses) must be kept to a minimum as the cells typically react negatively by rounding up as shown in the images in Figure 2.2c and d. The use of neutral density filters, bright high-quantum yield fluorophores, the reduction of laser power, and simply restricting to a minimum time that one looks at a specimen before beginning a time-lapse recording will help to reduce phototoxicity.

Another issue related to illumination that is generally encountered with live-cell imaging is known as *unintentional photobleaching*, which is the loss of emitted light by the permanent destruction of the fluorophores. Some fluorescent probes used in biological applications photobleach quicker (e.g., blue fluorescent protein, CFP,

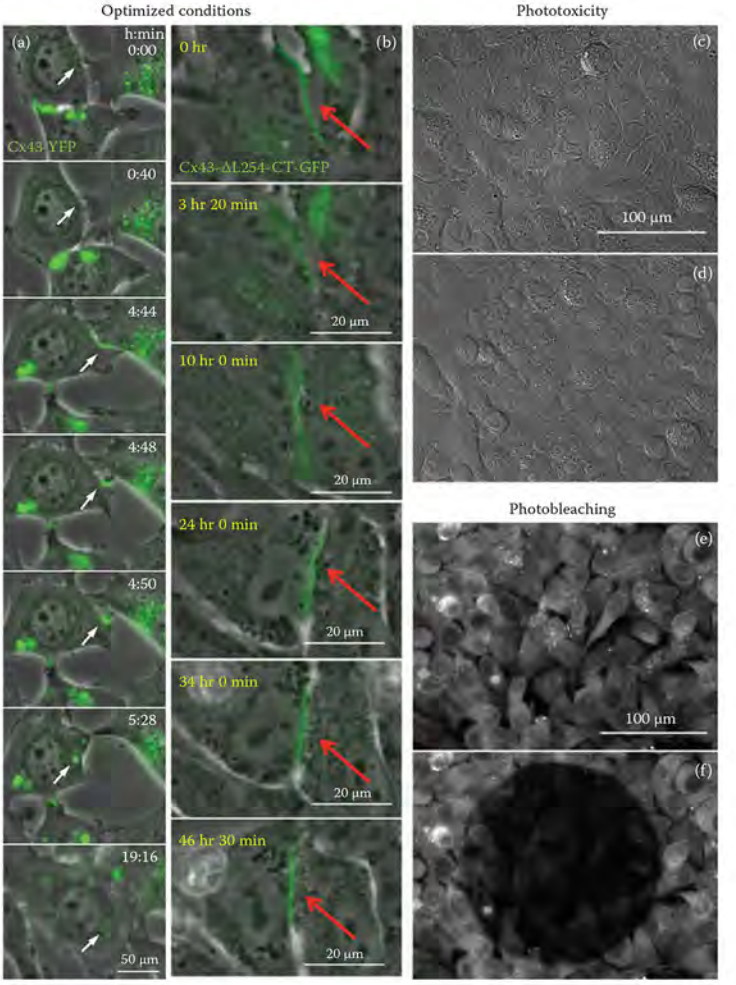

FIGURE 2.2 **(See color insert.)** Optimized imaging conditions and negative effects of excitation light. Optimizing cell culture and imaging conditions allow the cells to reside physiologically active for many hours as shown on the selected still images of the extended time-lapse recordings of the cells (over 20 hours in (a) [Reproduced from Fong, J. T., R. M. Kells, A. M. Gumpert, J. Y. Marzillier, M. W. Davidson, and M. M. Falk, *Autophagy*, 8, 794–811, 2012. With permission.] and over 46 hours in (b) [Reproduced from Fong, J. T., R. M. Kells, and M. M. Falk, *Mol Biol Cell*, 24, 2834–48, 2013. With permission.]) expressing wild type Cx43-eYFP (in (a)) and an internalization-deficient mutant (Cx43-ΔL254-CT-eGFP) (Fong, Kells, and Falk 2013.). Note the formation, internalization, and degradation of a gap junction plaque in (a), while the large internalization-deficient gap junction plaque in (b) stays in the membrane for the entire time of the recording. Phototoxicity resulting in rounded up cells (d) after exposing them to strong, short (blue) wavelength excitation light for several minutes. (c) The same area imaged before prolonged exposure. The loss of fluorescence intensity is due to unintentional fluorophore photobleaching resulting from prolonged exposure. The same area (e) before and (f) after exposure with the field diaphragm partially closed during the exposure time.

Lysotracker Red, Rhodamine) than others (e.g., eGFP, Alexa488, mCherry, mApple). An example is shown in Figure 2.2e and f. The cells stained with a fluorescently labeled antibody that decorates the plasma membrane were imaged right after selecting a region (Figure 2.2e), and again a few minutes later (Figure 2.2f). To demonstrate the significant loss of fluorescence emission, the field diaphragm was partially closed to restrict illumination to only the central portion of the imaging field. The diaphragm was then fully opened just before taking the second image. Again, avoiding unnecessary illumination in any form and selecting less sensitive and more stable probes may help to reduce this issue.

2.3 IMAGING TECHNIQUES

2.3.1 Wide-Field Microscopy

Wide-field and confocal fluorescence microscopy are standard imaging techniques which are routinely used in live-cell imaging, including gap junction research. Both techniques have their advantages and disadvantages and produce images of different appearance (see Figure 2.3a through c). This makes one technique preferable over the other depending on the research goal. More specialized imaging techniques such as total internal reflection fluorescence (TIRF) microscopy, a technique that only detects fluorescent signals in the immediate vicinity of the coverslip surface (up to a few hundred nanometers from the surface, see Section 2.7.2); and the now commercially available but costly superresolution and two-photon confocal microscope systems are not required for the investigation of connexins and gap junctions in living cells and are not further discussed here.

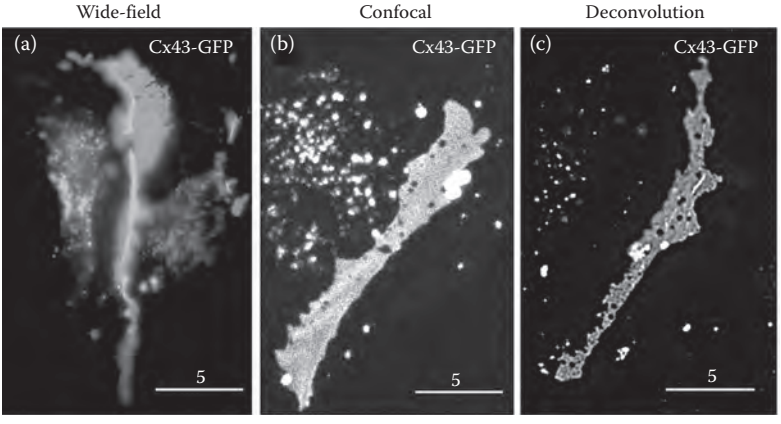

FIGURE 2.3 (See color insert.) Imaging techniques and image resolution. Gap junction plaques assembled from Cx43-GFP were imaged with (a, c) wide-field and (b) confocal microscopy. The Z image stack acquired in (c) was deconvolved postacquisition and a volume view was generated using mathematical image deconvolution algorithms. High primary image resolution achieved by high-quality, high NA oil immersion objectives is desirable and is required if the structural details of the gap junction plaques are to be resolved as shown for homomeric gap junction plaques assembled from

(*Continued*)

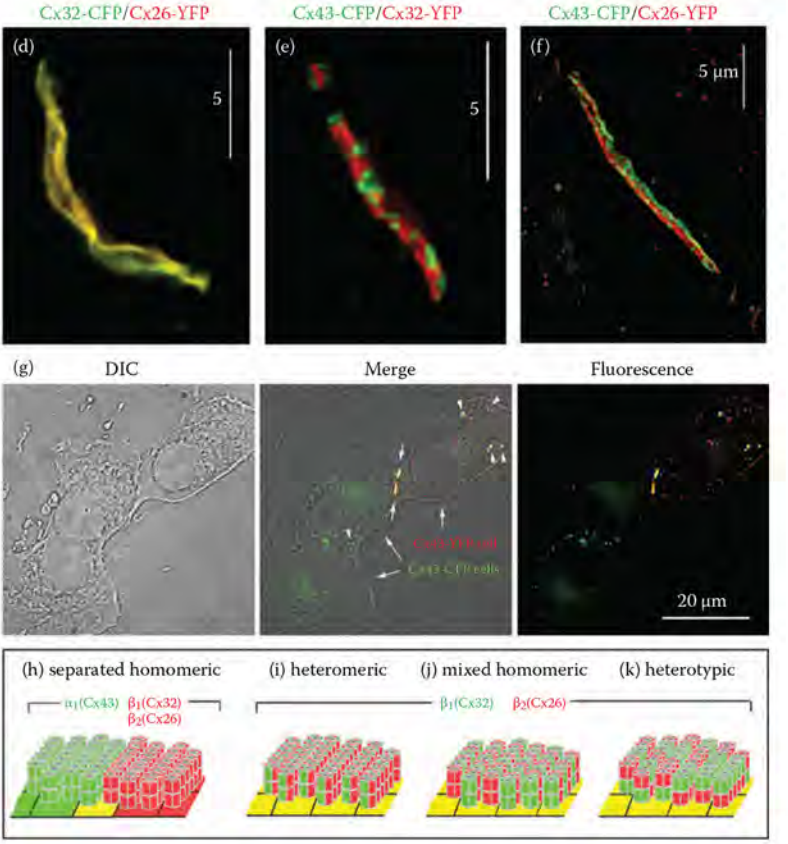

FIGURE 2.3 (CONTINUED) **(See color insert.)** Cx43-eCFP and Cx32-eYFP in (e), or Cx43-eCFP and Cx32-eYFP in (f) (Reproduced from Falk, M. M., and U. Lauf: High resolution, fluorescence deconvolution microscopy and tagging with the autofluorescent tracers CFP, GFP, and YFP to study the structural composition of gap junctions in living cells. *Microsc Res Tech*. 2001. 52. 251–62. Copyright Wiley-VCH Verlag GmbH & Co. KGaA. Reproduced with permission.) Individual connexins and gap junction channels (docked connexons) are too small to be resolved by light microscopy and appear yellow (the resulting color of merged green and red fluorescence) shown for a gap junction plaque assembled from Cx32-eCFP and Cx26-eYFP in (d) (Falk 2000a) and for heterotypic gap junctions assembled from Cx43-eCFP and Cx43-eYFP connexons shown in (g). (Reproduced from Piehl, M., C. Lehmann, A. Gumpert, J. P. Denizot, D. Segretain, and M. M. Falk, *Mol Biol Cell*, 18, 337–47, 2007. With permission.) The scheme in (h) through (k) depicts the resulting image color of different types of gap junction plaques.

As living cells are sensitive to the repeated intense light pulses required for imaging wide-field microscopes are often more compatible with live-cell imaging compared to confocal point scanners. As the whole field of view is imaged in a single exposure, the less intense light typically provided by a mercury-arc or a xenon lamp (now also strong light-emitting diode illumination systems) is sufficient.

2.3.2 Confocal Fluorescence Microscopy (Point Scanners and Swept Field/Spinning Disk)

Confocal microscopes that use pinholes to achieve confocality (the thickness of the focal plane that is imaged) collect only a single, 1–2 μm thin plane at a time. These microscopes need to systematically scan the field of view to acquire an image, a process that generally takes much longer and requires more intense illumination solely provided by a laser light source (Figure 2.3b). Commercially available spinning disk and swept-field confocal systems image multiple focal points simultaneously and are thus faster. This reduces excitation light intensity and time, yet also reduces confocality. Another advantage of wide-field systems beside the lower price tag is that the entire depth of view is captured and thus objects such as vesicles trafficking along microtubules (see Section 2.7.2), which move out of the focal plane, become blurry, but remain visible. In a confocal system, these vesicles become "lost" (are no longer captured) when moving out of the focal plane, which could lead to the false interpretation that they fused with the plasma membrane or another subcellular structure. Out-of-focus fluorescence blur can be reduced or eliminated by applying mathematical deconvolution algorithms that are built into most advanced imaging software packages commercially available today (compare Figure 2.3a and c). However, the technique requires collecting Z stacks of equally spaced images (collected at ≤0.2 μm distance) that again add imaging and exposure time, increase unintentional photobleaching, and increase file size. It also may generate image distortion, especially if faster moving objects are to be resolved. In our lab, the imaging of gap junctions and the postacquisition deconvolution were performed on a DeltaVision 283 imaging system (Applied Precision Inc., Issaquah, Washington). The ability to intentionally photobleach, photoconvert, and photoactivate the chromophores in defined image regions and the ability to convincingly detect the colocalization of the chromophores make confocal microscopy the preferred imaging system for these applications. A comparison of both imaging techniques mentioning a number of relevant pros and cons is given in Figure 2.4.

2.3.3 Imaging Gap Junctions with Different Imaging Techniques

In conventional light microscope systems (not superresolution), even at the highest magnification, the image resolution as defined by Rayleigh's law* depends on the wavelength of the light used for the excitation and is restricted to about 200 nm (e.g., 400 nm wavelength blue light). Thus, the fluorophores that are spaced less than this minimal distance normally cannot be resolved, as shown, for example, in Figure 2.3d and g for gap junction plaques assembled from heteromeric connexons (assembled from coexpressed Cx32-CFP [pseudocolored green] and Cx26-yellow fluorescent protein (YFP) [pseudocolored red]), and heterotypic gap junctions assembled between cocultured, Cx43-CFP (green) and Cx43-YFP (red) expressing

* $d = 1.22\lambda n/(2\text{NA})$; δ = smallest resolvable distance between two points; λ = wavelength of the excitation light in nm; n = refractive index (= 1.0 in air; 1.33 in water; 1.52 in immersion oil); NA = numerical aperture (an index indicating how much light an objective can collect; high NA = high resolution).

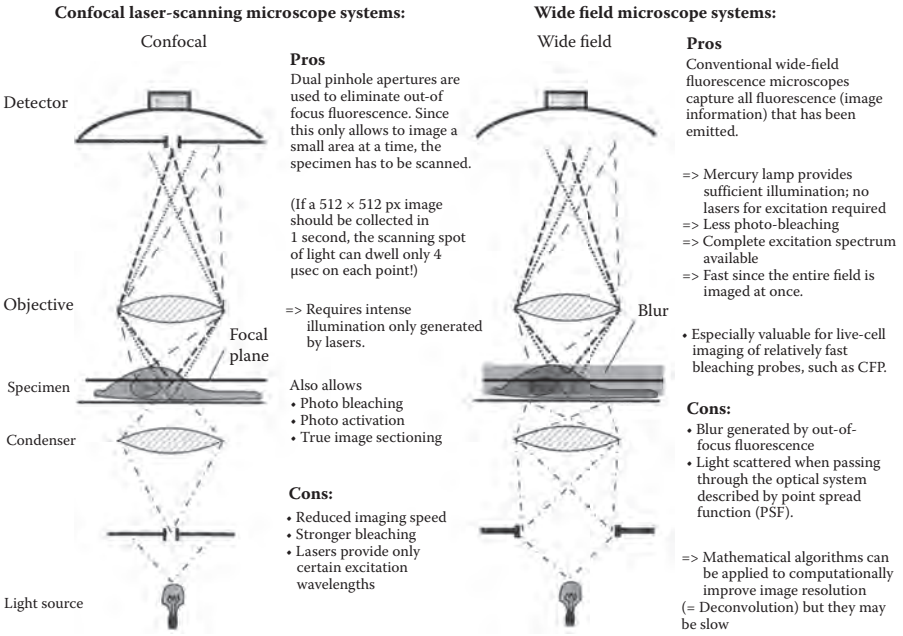

FIGURE 2.4 Pros and cons of wide-field and confocal microscopes. Both techniques have their positive and negative features that make both systems desirable dependending on the goal that one aims to achieve.

cells, respectively. In both cases, the gap junction plaques (depicted with arrows in Figure 2.3g) and the internalized annular gap junction vesicles (depicted with arrowheads) appear yellow in the merged images, the resulting color of the superimposed green and red fluorescent signals (see Section 2.10). Signal separation is simpler if the fluorophores are well separated as in the gap junction plaque assembled from Cx43-CFP and Cx32-YFP shown in Figure 2.3e in which homomeric, homotypic channels consisting of either connexin type formed large domains (red or green). If the domains are small, as in the gap junction plaque assembled from Cx43-CFP and Cx26-YFP shown in Figure 2.3f, high primary image resolution (high quality, color-corrected [apochromat] 60× or 100×, high NA), oil immersion objectives, and CCD cameras with sufficiently large photo chips (≥1024 × 512 px) are required. Domains smaller than the resolution limit (or two types of homomeric/homotypic gap junction channels placed next to each other akin to the field on a checkerboard) will not be resolved and will appear yellow. A schematic of different types of gap junction channels and the resulting merged image color is shown in Figure 2.3h through k. Note that a yellow stripe may appear on images of the plaques where red and green domains touch (as in Figure 2.3h) when both colors are detected by the same pixels (the ones located along the green/red fluorescence border line) on the CCD camera photo chip. Also note that the mixed homomeric (as depicted in Figure 2.3j) and heterotypic channels (as depicted in Figure 2.3k) will also appear yellow.

2.4 FLUORESCENT PROBES

The imaging of gap junctions in live cells requires fluorescent tagged connexins for detection in the microscope. Cloning the cDNA of a fluorescent protein or other probe in the frame with the connexin cDNA sequence and expressing the resulting fusion protein in cells can achieve this. It should be noted that antibody staining in general is not suitable for live-cell imaging because the use of antibodies requires that the cells be fixed and their membranes be permeabilized (unless microinjected into cells; not a trivial process and only a relatively small number of cells can be labeled at a time).

2.4.1 Green Fluorescent Protein and Derivatives

GFP and its derivatives today are the most commonly used fluorescent probes. Its discovery and development into a user-friendly live-cell fluorescence probe* was honored with the awarding of the Noble Prize in Chemistry in 2008 to Osamura Shimomura, Martin Chalfie, and Roger Y. Tsien. GFP's ability to autofluoresce (emit green fluorescent light when excited with blue light) and its inert, noninvasive properties resulting in a cytoplasmic expression in mammalian cells (Figure 2.5f) have significantly contributed to the enormous popularity of this probe. At present, over 53,000 papers come up in MedLine when *green fluorescent protein* is searched for. Not surprisingly, this remarkable probe has revolutionized and revitalized modern cell biology. Interestingly, a whole toolbox of monomeric fluorescent proteins emitting from blue to far red are now available (Shaner et al. 2004, 2007) allowing for the simultaneous detection of several proteins of interest in living cells. For the purposes of live-cell imaging, cells can be either transiently transfected with a fluorescent connexin prior to imaging or cell lines that stably express fluorescent connexins can be used.

2.4.2 Tagging Connexins with Green Fluorescent Protein and Other Fluorescent Proteins

Tagging connexins on their C-terminus (designated Cx-GFP) is normally well tolerated. C-terminal GFP-tagged connexins traffic normally (see Section 2.7) and assemble into typical gap junctions (Figure 2.5a) that are functional in respect to dye transfer (Falk 2000a; Jordan et al. 1999) and exhibit only minor alterations in electrophysiological channel characteristics (Bukauskas et al. 2000). Indeed, enough space is available in a connexon for six GFP tags placed on the C-terminus to simply extend a gap junction channel into the cytoplasms (Figure 2.5b) (Falk 2000a). The length of the linker that connects the connexin and the fluorescent

* GFP was isolated from the southwest Pacific jellyfish *Aquorea victoria*. In an effort to enhance the proteins as a fluorescent live-cell compatible probe, codon usage was optimized for mammalian applications, dimerization tendency was removed, and brightness and stability were enhanced (designated eGFP). All fluorescent protein tags that have been used in this chapter were purchased from Promega Inc., and are designated eCFP, eGFP, eYFP (yellow fluorescent protein), etc.

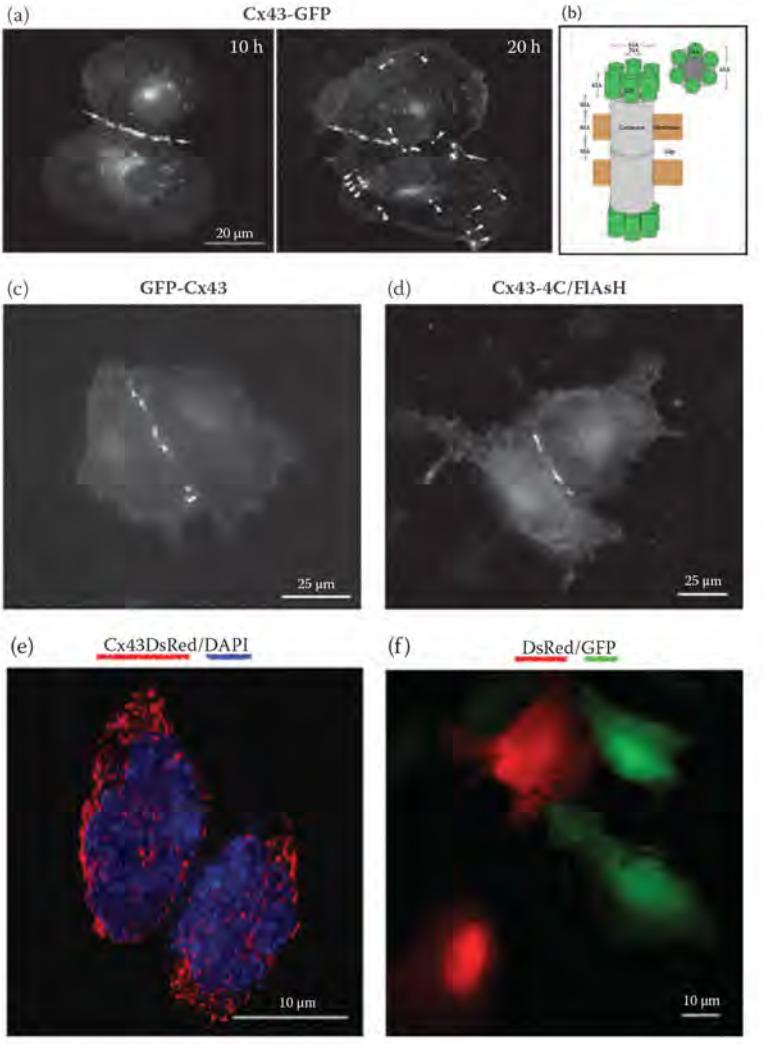

FIGURE 2.5 **(See color insert.)** Fluorescent probes. (a) Gap junctions assembled from Cx43 tagged with eGFP on the C-terminus imaged 10 and 20 hours posttransfection. (b) A schematic of a gap junction channel assembled solely from GFP-tagged connexins drawn to scale depicting that enough space is available in a connexon to spatially accommodate six C-terminally located GFP tags. (Reproduced from Falk, M. M, *J Cell Sci*, 113, 4109–20, 2000. With permission.) (c) Cx43 tagged with eGFP on the N-terminus also allows the nassembly of gap junction plaques, but these channels are not functional (Laird et al. 2001). (d) Gap junctions assembled from tetracysteine-tagged Cx43 and stained with FlAsH reagent (Gaietta et al. 2002). Cx43 tagged with the original red fluorescent protein, (e) DsRed; an obligate tetrameric protein, does not assemble into gap junctions and accumulates in the ER and the Golgi region while (f) DsRed expressed alone behaves inert and highlights the cytoplasm similar to GFP. (Reprinted from *FEBS Lett*, 498, Lauf, U., P. Lopez, and M. M. Falk, Expression of fluorescently tagged connexins: A novel approach to rescue function of oligomeric DsRed-tagged proteins, 11–5, Copyright (2001), with permission from Elsevier.)

protein sequence and its amino acid composition (providing more flexibility or rigidity) is likely to influence how well the fusion protein behaves. We have previously constructed a seven amino acid-long linker (including two central proline residues between the C-terminus and the GFP [Ala-Asp-*Pro-Pro*-Val-Ala-Thr]) with good results (Falk 2000a). It should be noted that fluorescent tags similar in size and conformation to GFP, such as CFP, YFP, mApple (and other color derivatives), or Dendra2 (see Section 2.8.2) and mEOS are similarly tolerated when placed on the C-terminus of the connexins (see Figures 2.2a, 2.3d through g, 2.7c,e, 2.9e through g, 2.10f,g and 2.11d).

2.4.3 Potential Issues Related to Size and Location of the Tag

Despite its popularity, a few drawbacks of GFP and other fluorescent color variants need to be considered in terms of gap junction research. First, GFP is a 238 amino acid, 27 kDa protein that folds into a can-shaped 4.2 × 2.4 nm structure. Several connexins (including Cx23, 25, and 26) have a lower molecular weight compared to GFP, and all others have a comparable molecular weight or are little more than two times of the molecular weight (Cx62 being the largest known connexin). Thus, tagging connexins with GFP and GFP derivatives may potentially have a negative impact on the normal behavior of connexins, and this should be considered. Indeed, we do know of at least one significant difference between untagged and C-terminal-tagged connexins. Gap junction plaques assembled from endogenously or exogenously expressed untagged Cx43 in general are much smaller than plaques with a GFP tag on the Cx43 C-terminus (see Figures 2.6d and 2.12a compared to images of plaques assembled from Cx43-GFP). The tag is known to prevent the Cx43-GFP fusion protein from interacting with the membrane scaffolding protein, zonula occludens 1 (ZO-1), a regulatory protein believed to control plaque size (Hunter et al. 2005; Rhett and Gourdie 2012). The last C-terminal amino acid residues of Cx43 (and of other connexins) bind into a pocket of the ZO-1 PDZ2-domain (Chen et al. 2008). Thus, any addition to the connexin C-terminus will most likely prevent a Cx/ZO-1 interaction (reviewed by Thévenin et al. 2013). This change in gap junction behavior must be considered when performing relevant experiments.

Unexpectedly, placing GFP on the N-terminus of the connexins (designated GFP-Cx) also allows the assembly of gap junction plaques (Figure 2.5c); however, these channels are not functional (Laird et al. 2001), likely because the N-terminal domains of the connexin fusion protein subunits are misfolded. As we know from the crystal structure of a Cx26 gap junction channel, the N-terminal domains of the connexin proteins are located inside the channel and form the channel vestibule (Maeda et al. 2009; reviewed by Thévenin et al. 2013). As the diameter of the channel pore of a connexon only measures ~1.5 nm, not enough space for even a single GFP tag is available inside a gap junction channel, likely forcing the connexin N-terminus and the attached GFP tag outward into the cytoplasm (discussed by Thévenin et al. 2013). We know that the N-termini of the connexins harbor a flexible hinge (Kalmatsky et al. 2012, 2009; Purnick et al. 2000) that may facilitate such a conformational

rearrangement. Albeit impaired channel function, N-terminal-tagged connexins may be helpful tools in addressing certain questions.

2.4.4 Other Fluorescent Probes: HaloTag and Tetracysteine Tags

More recently, a novel protein-labeling technology based on a modified bacterial haloalkane dehalogenase, HaloTag (Los et al. 2008) (commercially available from Promega), has been developed that may provide additional versatility to the fluorescent protein–connexin toolbox. However, at 34 kDa, the HaloTag protein is even larger than the GFP. Additionally, and opposed to the GFP, the N-and C-termini are not next to each other in the HaloTag protein structure but located on opposite ends (Los et al. 2008), potentially creating additional issues if the HaloTag is to be placed inside the connexin sequence. Very recently, the first paper describing a HaloTag-tagged connexin, Cx36 has been published (Wang et al. 2015).

Another, much smaller class of tags are the biarsenical tetracysteine (4C) peptide tags (Griffin et al. 1998) that can allow real-time tracking of connexins and gap junctions in living cells (Figure 2.5d) (Boassa et al. 2010; Gaietta et al. 2002). A big advantage of these tags is their small size (only 6–12 amino acids) compared to fluorescent proteins, and they have been successfully placed inside the Cx43 C-terminal tail (Boassa et al. 2010). However, 4C tags are nonfluorescent, and the cells need to be stained for the tagged fusion proteins to become detectable. Biarsenical labeling reagents, FlAsH (green), and ReAsH (red), which bind to the uniquely arranged cysteine residues of the 4C tags, are commercially available as vector and staining kits (Life Technologies/Invitrogen). A comprehensive comparison of fluorescent protein and 4C tags has been published by Falk (2002).

2.4.5 Photoactivatable Fluorescent Proteins

Photoactivatable fluorescent tags that can be switched on and off by pulsing them with different distinct wavelengths of light have also been developed (reviewed by Lippincott-Schwartz and Patterson 2009; Shcherbakova et al. 2014). However, they are only useful for dynamic studies if the location of the protein of interest (connexin) is known, as the tagged proteins are not initially visible.

Taken together, fluorescent tags have made the investigation of connexins and gap junctions in living cells possible. In general, fluorescent tags are well tolerated when placed on the C-terminus of Cx43 and other connexins; however, not all connexins have been investigated as fluorescent protein fusion constructs. Due to the size and the potential aberrant effects of fluorescent tags, it is always advisable to conduct follow-up studies of untagged connexins using anticonnexin-specific antibodies. Indeed, the first available red fluorescent protein, DsRed, now known to be an obligate tetrameric protein, completely prevented gap junction formation and caused Cx43-DsRed and other DsRed-tagged connexins to aggregate in the endoplasmic reticulum (ER) (Lauf et al. 2001) (Figure 2.5e), even though DsRed expressed by itself behaved inertly similarly to GFP (Figure 2.5f).

2.5 GAP JUNCTION/CONNEXIN LOCALIZATION: IS THE FLUORESCENT PUNCTUM A GAP JUNCTION?

2.5.1 Cytoplasmic and Plasma Membrane Markers, Combined Differential Interference Contrast/Phase Contrast and Fluorescence Illumination

When gap junctions are abundantly expressed they typically appear as puncta and lines in the plasma membranes outlining the periphery of cells (as, e.g., in Figures 2.6d,f, 2.12a, and c). However, when the gap junctions are scarce, small, and not clearly appearing as dashed lines (as, e.g., in Figure 2.9a), it may be difficult to differentiate the gap junction plaques from the cytoplasmic connexin-containing structures (secretory vesicles, internalized annular gap junctions, inclusion bodies created by overexpression, etc.). Staining the plasma membrane or the cytoplasm with a second fluorescent stain may resolve this concern. In Figure 2.6, several examples in live

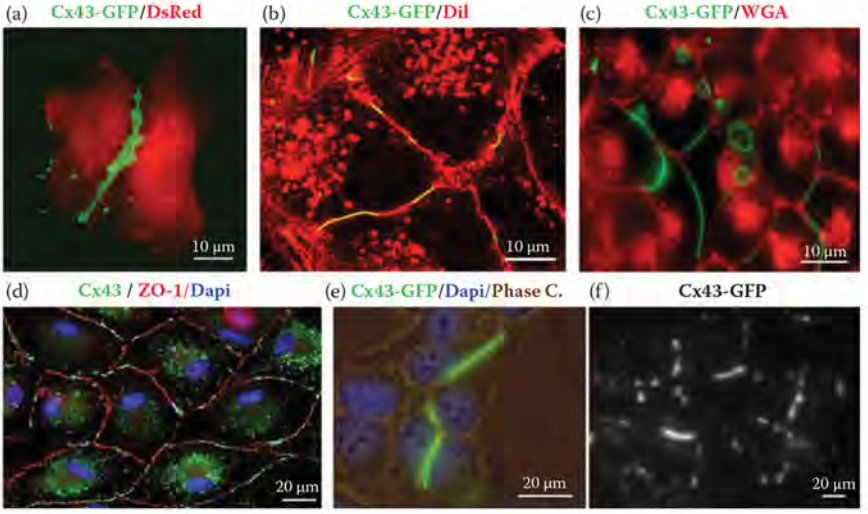

FIGURE 2.6 **(See color insert.)** Identification of gap junction plaques. To differentiate gap junctions from intracellular connexin-containing structures, it may be helpful to stain the cytoplasm by coexpressing an additional untagged fluorescent protein (in this case, DsRed), by staining the plasma membrane with membrane specific dyes such as (b) DiI (Reproduced from Falk, M. M., S. M. Baker, A. M. Gumpert, D. Segretain, and R. W. Buckheit III, *Mol Biol Cell*, 20, 3342–52, 2009. With permission.) or (c) WGA (With kind permission from **Springer Science+Business Media**: *J Membr Biol*, Degradation of endocytosed gap junctions by autophagosomal and endo-/lysosomal pathways: A perspective, 245, 2012, 465–476, Falk, M. M., J. T. Fong, R. M. Kells, M. C. O'Laughlin, T. J. Kowal, and A. F. Thevenin.), by staining in addition a membrane-localized protein, such as ZO-1 as in (d) (From Nimlamool, W., R. M. Kells Andrews, and M. M. Falk, *Mol Biol Cell*, 26, 2015. With permission.), or by acquiring and merging (e) phase contrast/DIC white light and fluorescent images. (Reproduced from Falk, M. M, *J Cell Sci*, 113, 4109–20, 2000. With permission.) Note that all the approaches shown with the exception of (d) are compatible with living cells.

(2.6a through c) and fixed cells (2.6d through f) are shown. The coexpression of a second fluorescent protein (not tagged to another protein) will label the cytoplasm (Figure 2.6a). Staining the cells for a few minutes with 1,1′-Dioctadecyl-3,3,3′,3′-tetramethylindocarbocyanine perchlorate (DiI) (a red lipid probe), fluorescent-labeled wheat germ agglutinin (WGA), or another commercially available lipid/plasma membrane marker before imaging will directly label the plasma membranes (Figure 2.6b and c). This can also be achieved in fixed cells by indirectly labeling the plasma membrane by costaining a plasma membrane-localized protein such as ZO-1, cadherin, catenin, etc. (Figure 2.6d). Finally, acquiring and merging phase contrast/differential interference contrast (DIC) white light images with fluorescent connexin images will not only demonstrate the plasma membrane localization, but also identify the location of other connexin-positive structures (see Figures 2.6e, and 2.9a through c). This can be done both in living as well as in fixed cells, and even the cell nuclei can be stained in the living cells if the DAPI label is replaced with a membrane-permeable chromatin dye such as Hoechst 33342.

2.6 GAP JUNCTION PLAQUE DYNAMICS

2.6.1 Plaque Structure, Fusion and Splitting, Spatial Movement of Gap Junctions, and Connexin-Free Junctional Membrane Domains

Time-lapse recordings of gap junctions can provide detailed information about plaque structure and dynamics when images are acquired at high primary magnification/resolution. Gap junctions can be oriented in two principal directions when viewed under a microscope depending on the cell morphology. If the lateral membranes of cells in a monolayer are oriented perpendicular to the image plane (e.g., found in general in polarized cells such as Madin–Darby canine kidney [MDCK] cells), the gap junction plaques will appear as lines and puncta providing an edge-on view (Figure 2.7a, top). If the cells are (partially) growing on top of each other (often found in HeLa and other non-contact inhibited cancer cells), the lateral membranes may be oriented more horizontal to the image plane, allowing a surface view (en face) of a gap junction plaque (Figure 2.7a, bottom). All examples of gap junctions shown in Figure 2.7b through f are en face views. Figure 2.7b depicts the structural dynamics of a gap junction plaque over time (55 minutes). Note the undulating edges, the deep invaginations, the more or less dark spherical connexin-free junctional membrane domains within the fluorescent plaque, and the drastic rearrangement of the two-dimensional shape of the plaque over time. Figure 2.7c depicts the fusion of two gap junction plaques by laterally moving in the plasma membranes. Note how the plaques move closer and closer together and suddenly fuse over their entire length. Figure 2.7d depicts the splitting of a gap junction plaque. In contrast to plaque fusion, the plaque portion that splits away slowly separates from the main plaque region with the connecting region becoming thinner and thinner before finally separating (comparable to an overstretched rubber band). Figure 2.7e depicts the fusion of plaque domains assembled from Cx43-CFP-labeled channels (green) present in a plaque that otherwise consists of Cx26-YFP-labeled channels (orange red; also

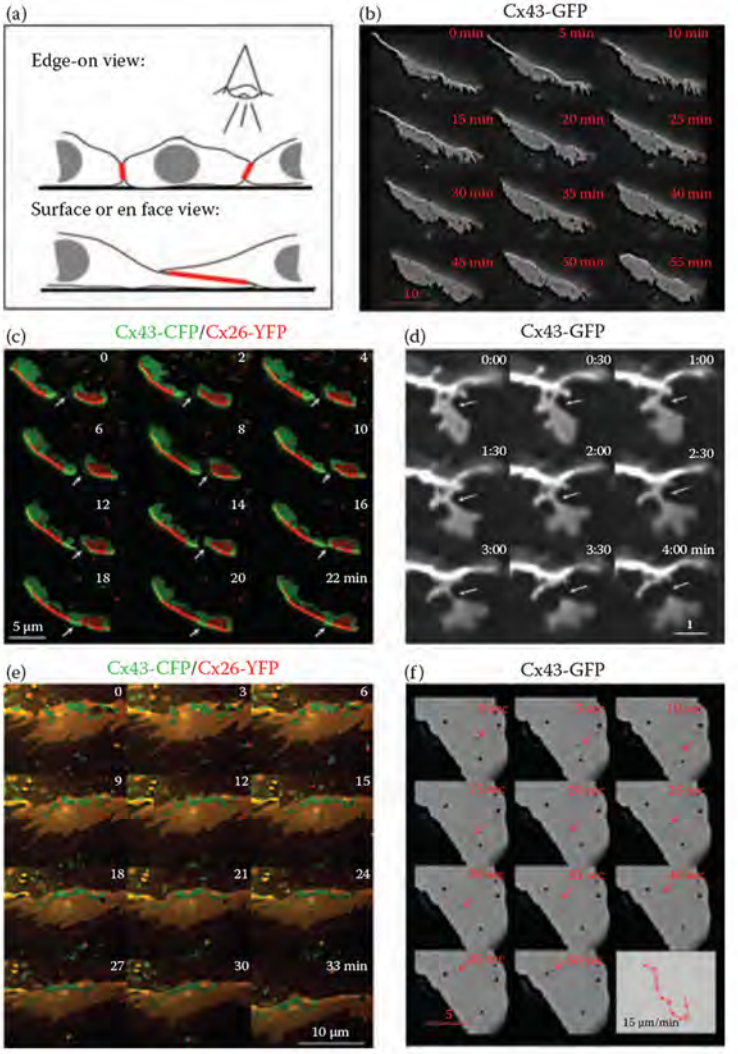

FIGURE 2.7 **(See color insert.)** Gap junction plaque dynamics. (a) Edge-on and en face surface views of gap junctions visible in cells depicted schematically. (b) Gap junction plaques are quite dynamic assemblies that structurally rearrange significantly over time. The gap junction plaques can fuse (depicted with arrows in c), split (depicted with arrows in d); (e) the domains (in this case, assembled from Cx43-eCFP [green]) in a gap junction otherwise consisting of Cx26-eYFP (orange/red) can split and fuse (Reproduced from Lopez, P., D. Balicki, L. K. Buehler, M. M. Falk, and S. C. Chen, *Cell Commun Adhes*, 8, 237–42, 2001. With permission.), and (f) connexin-free junctional domains (spherically shaped domains not containing connexins or gap junction channels and thus appearing dark) can move rapidly and saltatory throughout the gap junction plaques (Falk et al. 2009). While the structural rearrangements in (b) through (e) are relatively slow (in the minute range), the connexin-free junctional membrane domain dynamics (in f) can be fast (in the second range) requiring much shorter imaging intervals.

see the domain dynamics in the plaques shown in Figure 2.7c). These structurally dynamic rearrangements of the gap junctions are relatively slow in motion and can be detected by acquiring an image every 0.5–5 minutes. In contrast, the dynamics of connexin-free junctional membrane domains (not containing gap junction channels and appearing as dark, relatively spherical domains within the gap junction plaques [Falk et al. 2009] can rapidly move, requiring faster image acquisition [1–10-second intervals]). The tracking of one of these domains, moving 15 μm in 1 minute, is depicted in Figure 2.7f. In general, if the cells tolerate the extra excitation light and the probe is not rapidly bleaching, taking too many images is better than spacing them too far apart as rapid movements may become difficult or impossible to track with confidence (see, e.g., Section 2.7). Cutting out redundant images (as done in the collages shown in Figures 2.2a, 2.7b through f, 2.9f,g, 2.10a through g, 2.11b, and e, and in time-lapse movies) is always possible. Taken together, these recordings of gap junctions demonstrate that the channels within the gap junctions remain mobile resulting in a change of morphology of the plaques over time, to fuse and split, and to move throughout the plaque due to the fluidly arranged lipids that surround each gap junction channel (see Falk et al. 2009).

2.7 TRAFFICKING/SECRETORY PATHWAY

If Cx43-GFP fluorescence is imaged as soon as the fluorescence becomes detectable in cells (approximately 4–6 hours after transient transfection), a fluorescent haze highlighting the cytoplasm is detectable (suggesting ER localization) that then accumulates in the perinuclear regions (suggesting Golgi localization, labeled with arrows) before the gap junctions become visible (Figure 2.8a, 4 and 5 hours). Next, small gap junction plaques appear, which grow in size over time (Figure 2.8a, 5–20 hours, labeled with arrowhead). As described earlier, C-terminal-tagged connexins that are unable to interact with ZO-1 may grow very large and may occupy the entire lateral membrane space (as in Figure 2.8a, 40 hours). At this time, large, bright-fluorescent, spherical structures appear in the cytoplasm of some cells, suggestive of internalized gap junctions (Figure 2.8a, 20–80 hours; also compare Figure 2.5b, 20 hours). In a transient transfection, as shown in Figure 2.8a, new protein biosynthesis ceases after 24–48 hours due to the degradation of the cDNA, and no new Cx43 protein is biosynthesized at this time. As the gap junctions turn over, fewer and fewer remain (Figure 2.8a, 60 hours), and finally only internalized gap junctions and gap junction degradation products remain visible (Figure 2.8a, 80 hours).

2.7.1 Colocalization with Relevant Compartment Markers

As is typical for membrane proteins, Cx43 has been shown to cotranslationally insert into the ER membranes and to traffic via the Golgi apparatus to the plasma membrane (Koval 2006; Falk and Gilula 1998; Falk et al. 1997, 1994; Laird 1996; Musil and Goodenough 1993). We demonstrated Cx43-GFP colocalization by staining fixed

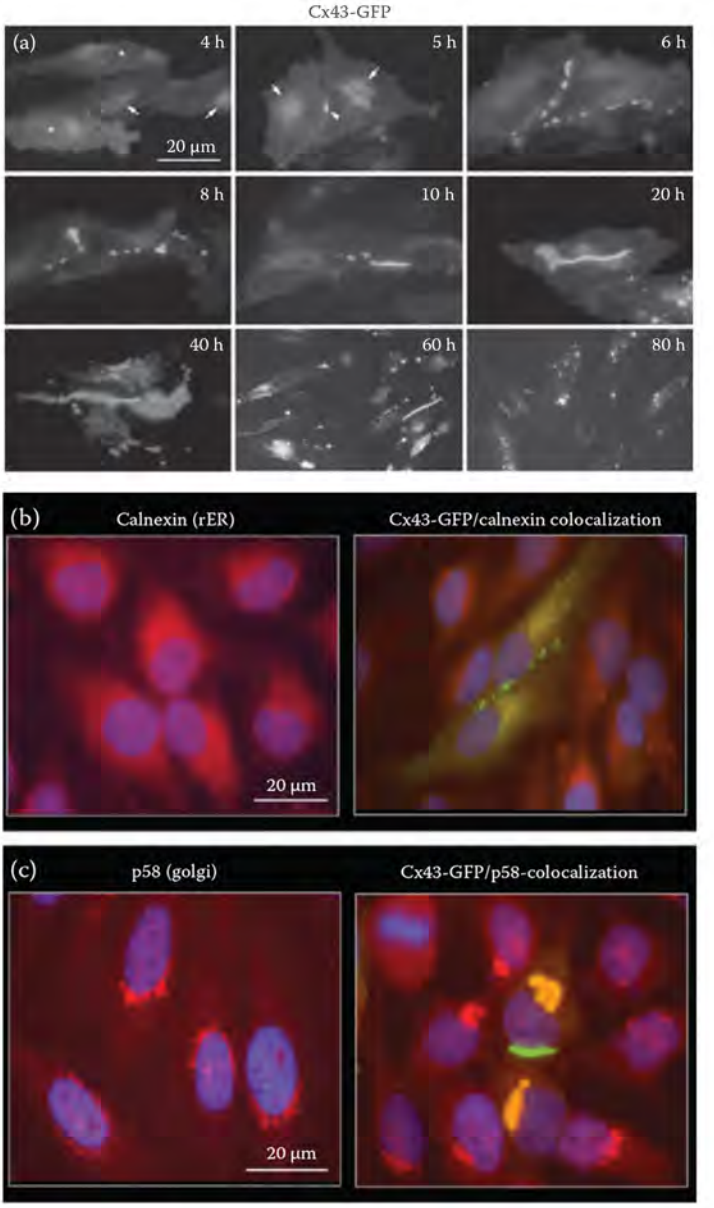

FIGURE 2.8 **(See color insert.)** Connexins trafficking along the secretory pathway: Colocalization with relevant compartment markers. (a) The stages of Cx43-GFP expression in transiently transfected HeLa cells including Cx43-eGFP ER and Golgi localizations (depicted with arrows in the images acquired earlier after transfection, 4–5 hours), formation of plasma membrane gap junctions (depicted with arrowhead, 5–40 hour), and cytoplasmic gap junction degradation vesicles (AGJs, 6–80 h). (b, c) Cx43-eGFP ER and Golgi localizations confirmed by costaining with ER (calnexin) and Golgi (p58) marker proteins. (Reproduced from Falk, M. M, *J Cell Sci*, 113, 4109–20, 2000. With permission.)

Cx43-GFP expressing cells with ER (calnexin) and Golgi (p58) marker proteins, respectively (Figure 2.8b and c). This can also be achieved in living cells by coexpressing an ER or a Golgi marker protein that is tagged with another fluorescent protein, or by staining the ER and the Golgi with compartment-specific membrane-permeable live-cell probes such as ER-Tracker™ Blue-White DPX or Texas Red-labeled BODIPY® ceramide, respectively (Cat. Nos. E12353 and D7540, Invitrogen/Molecular Probes).

2.7.2 Trafficking along Microtubules

Cx43 connexons have been shown to traffic from the Golgi to the plasma membrane in secretory vesicles that migrate along microtubules driven by a kinesin motor protein (Fort et al. 2011; Shaw et al. 2007; Lauf et al. 2002). Secretory vesicles, including connexon-containing vesicles, move fast, up to a micrometer per second (Fort et al. 2011; Falk et al. 2009; Lauf et al. 2002) (Figure 2.9a). To convincingly capture these fast saltatory movements, it is best to collect images in a rapid sequence, at least every few seconds; otherwise, reliable connexon-containing vesicle tracking may not be possible. Tracking analyses can be done in different ways based on time-lapse image sequences; however, labeling microtubules (by, e.g., coexpressing YFP tubulin) together with connexins may provide the most convincing results (Figure 2.9e through g). We, for example, have merged images of all time points after color coding each image in Photoshop® (Lauf et al. 2002) (Figure 2.9a). This highlights the vesicle tracks, as well as the directionality based on color coding. Several transport vesicles containing Cx43 connexons transitioning from the Golgi to the plasma membrane can be seen in the merged image shown in Figure 2.9b and c.

The path and the position of vesicles at each time point can also be shown by connecting the vesicle locations with lines as shown in Figure 2.9e and f. As mentioned earlier, it is imperative to collect images in rapid sequence to allow for reliable tracking. Figure 2.9f shows the track of a Cx43-CFP-containing vesicle (green) that moves along YFP-labeled microtubules (red). Note that at several times, the vesicle changes direction by jumping onto different microtubules, resulting in a curved, zigzag path.

Successfully imaging the fusion event of the secretory vesicles with the plasma membrane as well as observing the delivery of the protein cargo into the plasma membrane also require capturing several images per second (Schmoranzer et al. 2000; Toomre et al. 2000). TIRF microscopes commercially available today are ideal platforms for this task. The microscope system available to us in 2002 was not able to capture the images in such a rapid sequence, yet we were able to indirectly demonstrate vesicle/plasma membrane fusion and Cx43 connexon delivery (Lauf et al. 2002). Figure 2.9g shows a sequence of selected images captured at 15-second intervals depicting a small area of the plasma membrane of a Cx43-CFP (pseudocolored red)/YFP tubulin (pseudocolored green) expressing cell. Four Cx43-CFP vesicles (labeled with arrows) are piled up at the end of a microtubule extending into a filopodial plasma membrane extension (0:45 minutes). Three minutes later (3:45 minutes), only three vesicles remain; at 4:30 minutes, two

vesicles; at 4:45 minutes, one vesicle; and at 5:00 minutes, no vesicles remain. That the vesicles fused with the plasma membrane and did not move backward on the microtubule into the cytoplasm can be inferred from the fact that they are not visible on the microtubule closer to the minus end in any of the captured images. Indeed, two additional vesicles (on the same microtubule) do not move during the time of the recording, in this case, serving as convenient spatiotemporal markers.

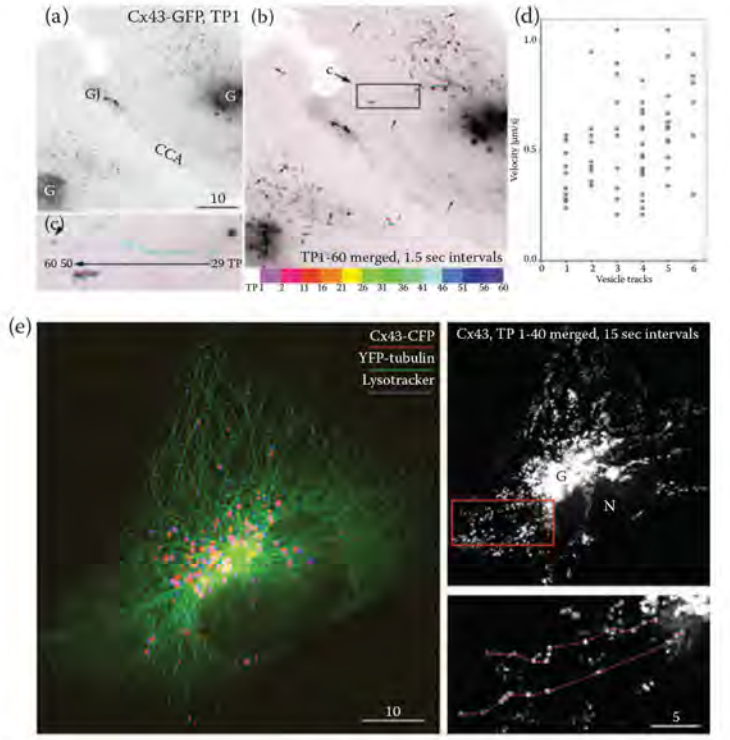

FIGURE 2.9 (See color insert.) Connexins trafficking along the secretory pathway: Trafficking along microtubules. To demonstrate the trafficking of connexons from the Golgi to plasma membrane, Cx43-eGFP-expressing HeLa cells were imaged at 1.5-second intervals. Time point 1 image (black and white inverted for contrast enhancement) is shown in (a). Each time point image was inverted and pseudocolored according to the color scheme shown in (b), and the colored images were merged resulting in vesicle tracks in which the directionality is indicated by the color coding. A selected track is shown in (c). The traveled distance measurements of six individual vesicles are shown in (d). (e) A HeLa cell expressing Cx43-eCFP and YFP-tubulin, and in addition stained with the live-cell compatible acidophilic stain, LysoTracker red (labeling lysosomes), was imaged every 15 seconds over time; the Cx43 channel images were merged, and the tracks of two Cx43-containing transport vesicles moving along microtubules were marked on the merged image insert. (Reproduced from Lauf, U., B. N. Giepmans, P. Lopez, S. Braconnot, S. C. Chen, and M. M. Falk, *Proc Natl Acad Sci U S A*, 99, 10446–51, 2002. With permission.)

(*Continued*)

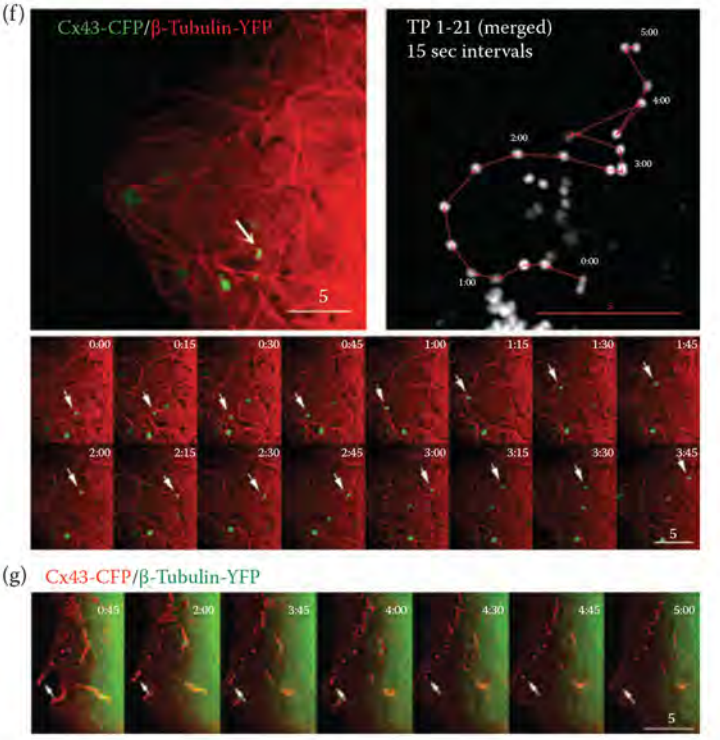

FIGURE 2.9 (CONTINUED) **(See color insert.)** Connexins trafficking along the secretory pathway: Trafficking along the microtubules. (f) A Cx43-eCFP-containing vesicle traveling along a curved microtubule (visualized by β-tubulin-YFP expression) and transitioning between different microtubules is depicted by outlining the traveled track with lines connecting the positions of the vesicle for each time point on the merged Cx43-eCFP channel image. The position of the vesicle at each time point is marked in the collage. (g) The delivery of Cx43-eCFP connexons packaged in transport vesicles into the plasma membrane inferred by the disappearance of the vesicles one after the other (marked with arrows) on the selected still images of a time-lapse recording of a Cx43-eCFP and β-tubulin-YFP-expressing HeLa cell. (Reproduced from Lauf, U., B. N. G. Giepmans, P. Lopez, S. Braconnot, S. C. Chen, and M. M. Falk, *Proc Natl Acad Sci U S A*, 99, 10446–51, 2002. With permission.)

2.8 PLASMA MEMBRANE DYNAMICS OF CONNEXONS AND GAP JUNCTIONS

2.8.1 Intentional Photobleaching: Fluorescence Recovery after Photobleaching and Fluorescence Loss in Photobleaching

Several microscopy-based techniques using living cells have been developed to investigate the dynamics of proteins in cells and can be applied to the study of connexins, connexons, and gap junctions. In fluorescence recovery after photobleaching (FRAP), the fluorescence signal emitted by a fluorescent protein in a defined area (square,

bar, arbitrary shape) is intentionally permanently photobleached through the use of a strong laser (up to 100% power output). If the photobleached protein of interest is capable of diffusion (either throughout the cytoplasm if it is a soluble protein or in the membrane if it is a membrane protein) overtime, the bleached area will regain fluoresce because unbleached proteins will diffuse back into the bleached area. All biological fluorophores will eventually lose fluorescence when extensively excited (see Figure 2.2e and f), even probes such as GFP and YFP, which are quite resistant to photobleaching. Green-fluorescent probes in general were much easier to photobleach, as the argon ion lasers on conventional confocal microscopes (generating the blue 488 nm excitation line used to excite green fluorescent probes) have a much stronger energy output (approximately 50 mW) than the green-generating excitation line (543 nm, commonly used to excite red fluorescent probes) of helium/neon lasers (approximately 5 mW; the newest confocal microscope systems now have equally strong lasers). We have used this technique to demonstrate the diffusion of connexons in the plasma membrane (Figure 2.10a and b), to track the growth of the gap junctions, and to track the turnover of channels from the gap junctions (Falk et al. 2009,

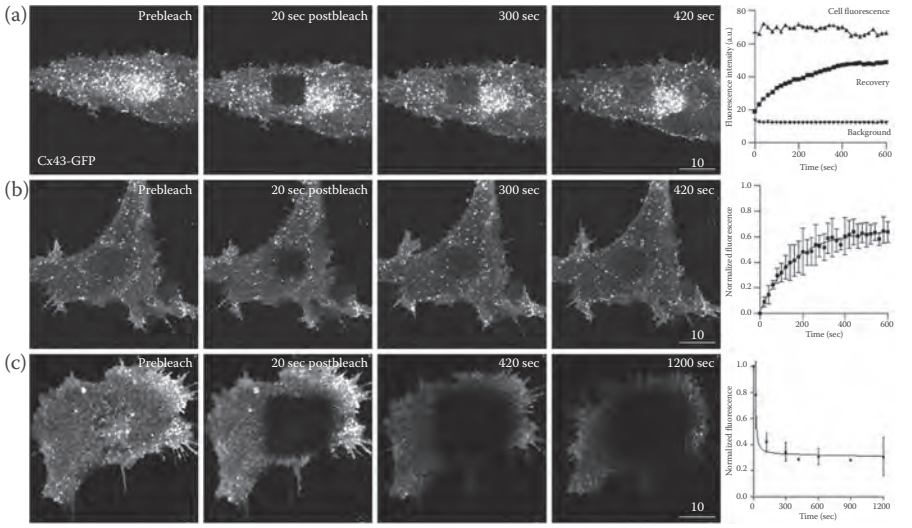

FIGURE 2.10 **(See color insert.)** Plasma membrane dynamics of connexons and gap junctions. (a, b, d, e) FRAP, (c) FLIP, and (f, g) Dendra2-photoconversion can be used to assess dynamics of connexons and gap junctions. (Reproduced from Lauf, U., B. N. Giepmans, P. Lopez, S. Braconnot, S. C. Chen, and M. M. Falk, *Proc Natl Acad Sci U S A*, 99, 10446–51, 2002. With permission.) In (a) and (b), the fluorescence in a $10 \times 10\,\mu m$ square in Cx43-eGFP-expressing HeLa cells was permanently photobleached using the laser of a confocal microscope. Note how the fluorescence "haze" indicative of dispersed plasma membrane-localized connexons recovers over time in the bleached area, while the intracellular, bright punctate fluorescence (probably predominantly inclusion bodies due to overexpression) in a remains largely immobile. In (c), the square area was repeatedly photobleached in 5-minute intervals resulting in an almost complete loss of cellular fluorescence over a 20-minute period.

(*Continued*)

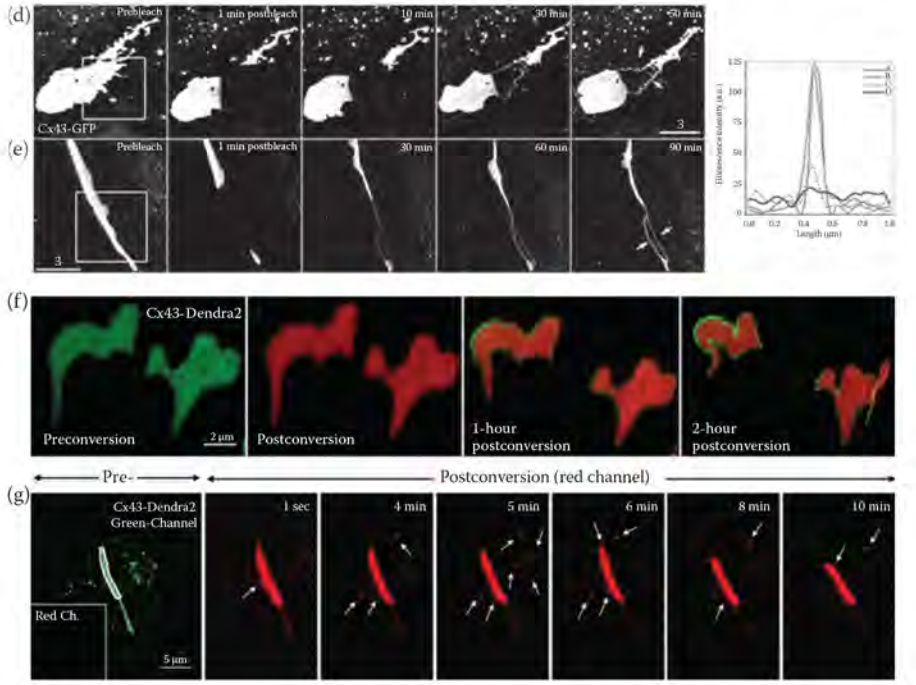

FIGURE 2.10 (CONTINUED) **(See color insert.)** Similarly, the fluorescence of the portions of Cx43-eGFP gap junction plaques (oriented en face in d, and edge on in e) was permanently photobleached. Note that the plaques recover a fluorescent rim of unbleached gap junction channels that grows wider over time, indicating that the newly synthesized channels are accrued to the outer edge of the gap junction plaques. (f) In a comparable approach, two gap junction plaques assembled from Cx43 tagged with Dendra2 were photoconverted from initially green to permanently red fluorescence using the 488 nm line of a confocal laser. Note that the plaques recover a rim of nonconverted green channels that grows wider over time, similar to the results obtained by FRAP experiments shown earlier. (g) Photoconversion also demonstrated that the vesicles (red, marked with arrows) were released from a photoconverted portion of an edge-on oriented gap junction plaque (outlined in white). (Reproduced from Falk, M. M., S. M. Baker, A. M. Gumpert, D. Segretain, and R. W. Buckheit III, *Mol Biol Cell*, 20, 3342–52, 2009. With permission.)

Lauf et al. 2002) (Figure 2.10d through g). Connexons/hemichannels delivered to the plasma membrane do not cluster into plaques comparable to docked gap junction channels. In confocal fluorescent images of Cx43-GFP expressing cells, the plasma membrane connexons appear as a fluorescent haze homogenously highlighting the plasma membrane (Figure 2.10a through 2.10c, panels labeled Prebleach). Note how the Cx43-GFP plasma membrane fluorescence in a photobleached square recovers as the connexons from surrounding unbleached membrane areas diffuse into the bleached area over time (Figure 2.10a and 2.10b). Interestingly, larger bright fluorescent Cx43-GFP-containing structures in the cytoplasm (internalized gap junctions and inclusion bodies) do not show a comparable dynamic behavior (Figure 2.10a).

In addition to FRAP, fluorescence loss in photobleaching (FLIP), a related technique, can be used to investigate connexon dynamics. In FLIP, the fluorescence in the defined area (e.g., a square) is photobleached repeatedly over time. If the proteins can laterally diffuse (such as connexons), the fluorescence will eventually be lost also outside of the bleached box, as the fluorophores diffuse into the boxed area and will be bleached in repeated bleach cycles. This technique demonstrates especially well the extent of dynamic movements either including the entire plasma membrane (as shown for connexons in Figure 2.10c) or being restricted to certain compartments (see Lauf et al. 2002).

When we permanently photobleached defined areas of gap junctions in Cx43-GFP expressing cells, the plaques recovered a fluorescent rim of unbleached channels clearly detectable within about 30 minutes. Fluorescent rims grew wider over time, indicating that the new channels were accrued along the edge of the Cx43-GFP gap junctions (Figure 2.10d depicts a plaque seen en face, Figure 2.10e depicts a plaque seen edge-on). Measuring the width of the fluorescent rim over time suggested a connexin half-life of approximately 2–3 hours, which corresponded to previously published data (Berthoud et al. 2004), to the Cx43 half-life calculated by Gaietta et al. (2002) who used successive FlAsH/ReAsH staining to demonstrate Cx43-based gap junction turnover, and to the experiments that used photoconvertible proteins (see Section 2.8.2) (Falk et al. 2009).

2.8.2 Photoconversion: Dendra2 and mEOS2

Photoconvertible fluorescent proteins such as Dendra2 and mEOS initially fluoresce green; however, they are photoconverted to a permanently red-emitting state when excited with moderate UV/blue light (Chudakov et al. 2007; Gurskaya et al. 2006). The photoconverted gap junctions assembled from Cx43-Dendra2 develop a progressive green outer rim of unconverted channels over time with similar kinetics to the photobleached gap junctions (Figure 2.10f). This technique also allowed us to directly visualize and quantify the vesicles generated by the internalization of the small plaque areas by photoconverting a portion of edge-on oriented gap junction plaques (Falk et al. 2009) (Figure 2.10g, released vesicles marked with arrows). Other more dynamic characteristics have been described for Cx43-based gap junction plaques (including an extremely fast, questionable turnover rate of only 2.7 minutes (Shaw et al. 2007), as it is not clear based on metabolic considerations how cells would maintain such a fast gap junction turnover rate), and for gap junctions assembled from other connexin types (Cx26) (Thomas et al. 2005). Fluorescent protein fusion tag and connexin type have also been reported to influence gap junction plaque stability (Stout et al. 2015).

When performing FRAP and FLIP experiments with connexins, it is important to keep the initial illumination to a minimum so as to not accidentally prebleach the fluorescent protein signal, and to make sure that the gap junctions do not move out of focus over time, as this may suggest falsified dynamic characteristics. This is especially important when using photoconvertible fluorescent proteins, as these easily convert unintentionally to red-emitting polypeptides if exposed to blue excitation light that is too strong. A detailed step-by-step protocol on how to successfully

photoconvert Dendra2- and mEOS-tagged proteins including gap junctions has been published by us previously (Baker et al. 2010). See also the methods sections in the manuscripts of Lauf et al. (2002) and Falk et al. (2009) for details on how to perform plasma membrane connexon and gap junction FRAP and FLIP experiments.

2.9 INTERNALIZATION AND DEGRADATION OF GAP JUNCTIONS

2.9.1 Imaging

Live-cell recordings of Cx43-GFP gap junctions demonstrated that the gap junction plaques and regions of plaques internalize as complete double-membrane spanning channels and do not split in half as is typical, for example, for adherens junctions (Ivanov et al. 2004a,b). The process generates cytoplasmic double-membrane gap junction vesicles (Falk et al. 2009; Piehl et al. 2007; Jordan et al. 1999), termed *annular gap junctions* (AGJs) or *connexosomes* (schemed in Figure 2.11a). Subsequent analyses have shown that clathrin as well as clathrin-endocytic machinery mediate this process (Xiao et al. 2014; Fong et al. 2013; Gumpert et al. 2008; Nickel et al. 2008; Piehl et al. 2007). Gap junctions assembled from other connexins have also been shown to internalize to form AGJs (Falk et al. 2014; Xiao et al. 2014; Johnson et al. 2013; Schlingmann et al. 2013). The process is quite impressive when captured in a time-lapse recording at high primary resolution with the image plane placed in the middle of a gap junction. In Figure 2.10b, the two gap junctions (a large and a small one, both labeled with arrows) are visible. Over time (89 minutes), the large gap junction successively bends toward the cytoplasm of the left cell, invaginates deeper and deeper and finally detaches forming a perfectly spherical AGJ in the cytoplasm of that cell, while the small gap junction resides undisturbed in the plasma membrane. The sphere is visible as a ring in a confocal and in a wide-field microscope when viewed at high primary magnification, as this generates only a thin focal plane (as seen in Figure 2.11b). However, Z sectioning will show the entire spherical morphology of the AGJs (Piehl et al. 2007). In addition, when combined with DIC white light illumination, the cell bodies become visible, demonstrating the translocation of the gap junction from its location in the plasma membrane into the cytoplasm of one of the connected cells (Figure 2.11c, depicted with arrowheads). Note that a new gap junction forms in the lateral membrane at a location proximal to that of the internalized gap junction (visible in the last image in Figure 2.11c, depicted with arrow).

2.9.2 Colocalization with Relevant Compartment Markers

The fate of endocytosed gap junctions and their degradation can be shown in living cells via colocalization by the coexpression of an endocytic marker protein tagged with a different fluorescent protein (as shown for LC3-GFP and Cx43-mApple as an example in Figure 2.11d), or by staining the subcellular compartments with specific live-cell probes (shown for proteolytic compartments stained with the acidophilic

live-cell marker, LysoTracker™ Red; Invitrogen/Molecular Probes) (Figure 2.11e). Other comparable probes specific for other subcellular compartments are available from Molecular Probes/Invitrogen (ER, Golgi, mitochondria, etc.) If the cells are fixed, antibodies directed against a relevant marker protein can be used (shown for p62/sequestosome1 [SQSTM1] and endogenously expressed Cx43 in pulmonary artery endothelial cells as an example in Figure 2.12d).

When investigating connexin and gap junction degradation, it is important to not only use markers for lysosomes because these structures participate in several different cellular proteolytic pathways (endo-/lysosomal as well as autophagosomal

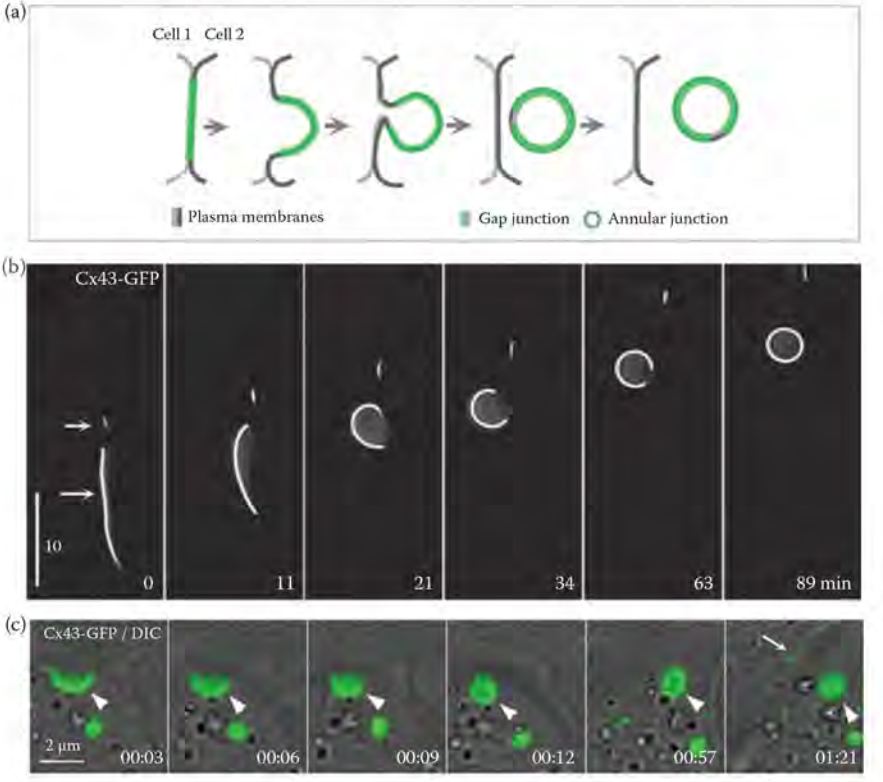

FIGURE 2.11 **(See color insert.)** Internalization and degradation of gap junctions. (a) Schematic depicting the internalization of gap junctions as complete double-membrane spanning channels. (Reproduced from Fong, J. T., R. M. Kells, A. M. Gumpert, J. Y. Marzillier, M. W. Davidson, and M. M. Falk, *Autophagy*, 8, 794–811, 2012. With permission.) The process leads to the formation of AGJ vesicles in the cytoplasm of one of the previously coupled cells. (b, c) The same process imaged by time-lapse microscopy in Cx43-eGFP-expressing HeLa cells (only the fluorescence is shown in b; the merged fluorescence and the DIC channels are shown in (c)). Note that the upper, small gap junction plaque in (b) (depicted with short arrow) does not internalize and remains in the plasma membrane; and that in (c), a new gap junction (depicted with arrow) is assembled at the location were the previous internalized gap junction plaque (depicted with arrowhead) was localized.

(*Continued*)

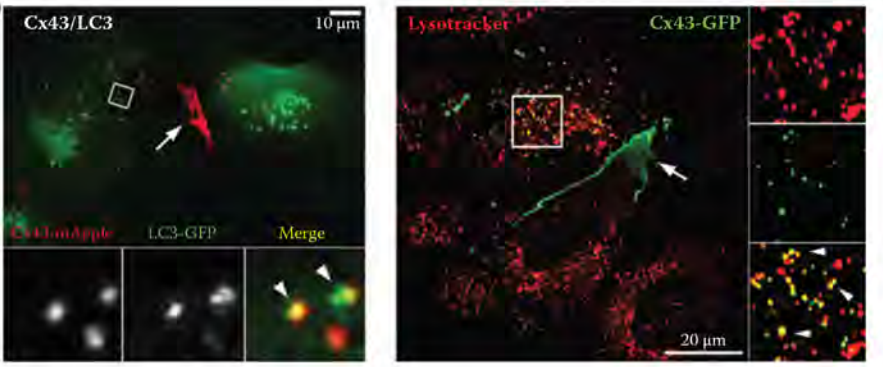

FIGURE 2.11 (CONTINUED) **(See color insert.)** Internalization and degradation of gap junctions. (d) Cx43-mApple-containing vesicles colocalize with LC3-GFP (a specific marker protein of autophagosomes) imaged in living cells, suggesting AGJ degradation via macroautophagy. (e) Cx43-eGFP-containing vesicles colocalize with LysoTracker Red-stained lysosomes imaged in living HeLa cells, further suggesting lysosomal-based degradation of AGJs. (Reproduced from Fong, J. T., R. M. Kells, A. M. Gumpert, J. Y. Marzillier, M. W. Davidson, and M. M. Falk, *Autophagy*, 8, 794–811, 2012. With permission.)

degradation). Indeed, AGJs have been shown as being degraded by macroautophagy, which converges with the lysosomal pathway (Bejarano et al. 2012; Fong et al. 2012; Lichtenstein et al. 2011; Hesketh et al. 2010). In addition, gap junctions have been presumed to also be degraded through the endo-/lysosomal pathway (Leithe et al. 2009; Qin et al. 2003; Laing et al. 1997), and misfolded connexin polypeptides can be degraded through the proteasomal pathway (Kelly et al. 2007; Laing and Beyer 1995). It is important to note that depending on the fluorescent probe that is used in degradation studies, the labeled degrading gap junctions may gradually lose their fluorescence because some GFP-types are sensitive to the low pH of the degradation compartments (see, e.g., the last still image in the time-lapse shown in Figure 2.2a).

2.10 FLUORESCENCE COLOCALIZATION

2.10.1 Tools and Techniques

Fluorescence colocalization analyses are typically performed on confocal microscopes.* Colocalization analysis is a powerful tool that can provide much information on the spatial interaction of connexins with binding partners throughout their life

* In contrast to a wide-field microscope, a conventional confocal microscope uses point illumination and a pinhole in an optically conjugate plane in front of the detector to eliminate out-of-focus emission light. As only the light very close to the focal plane is detected, the image's optical resolution, particularly in the sample depth direction (in Z), is much better than that of wide-field microscopes. However, as much of the light from the sample fluorescence is blocked at the pinhole and discarded, increased resolution is at the cost of decreased signal intensity, requiring light-intensive lasers for excitation and often long exposure times.

cycle (Interactome). In addition, temporal interactions of connexins with their binding partners may be resolved when colocalization analyses are performed in living cells. However, this technique also has the potential to produce significant false data when incorrectly performed. Colocalization is generally defined as two different fluorescently labeled proteins/molecules appearing in the same location on an image, which implies that they are interacting in some manner with each other. Colocalization will generate the resulting additive color by mixing both fluorescent labels in merged images (red colocalizing with green will result in yellow; blue colocalizing with green will generate cyan; red colocalizing with blue will give magenta; and colocalization of all three basic colors, red, green, and blue, will result in white* as in the examples shown in Figure 2.12a through d).

2.10.2 Potentially False-Positive Results

To avoid errors, first it is important that the pinholes on the confocal microscope are small (≤1 airy units), so that the image sections are thin (≤ 1 μm); otherwise, confocality is lost (the thickness of the image plane increases), and the fluorescent labels localized in the same spot in X and Y, but in different depths in Z, may falsely colocalize (see Lauf et al. 2001 for examples). Second, the primary image magnification and the resolution should be optimal (60/63× NA 1.4 plan-Apochromat oil-immersion objectives). Immersion oils with a refractive index that matches that of glass coverslips and objective lenses are essential to reduce the image distortion. Third, it is important to not overexpose the image, which may occur when using too much laser power or too long of an exposure time or by using autoimage settings of the imaging software package. Indeed, as the excitation and emission spectra of most commonly used biological labels and fluorescent proteins overlap, it is likely that at a given wavelength (for example, to excite GFP), another fluorescent protein (CFP, YFP, RFP) is excited to some extent as well (see Figure 2.12e). It is important to check for this "bleed-through" into other emission channels (photomultipliers) and adjust the exposure level to a point where no bleed-through is detectable. Figure 2.12f shows a purposely false colocalization of Rhodamine-labeled phalloidin that decorates the actin filaments. Rhodamine is a red fluorescent dye that also emits somewhat green if overexposed. This bleed-through into the green channel was acquired, the image brightness was enhanced post-acquisition using Photoshop software, and the red emission channel and the enhanced green bleed-through image were merged, resulting in a complete, but false colocalization signal! Reducing the laser excitation power and the exposure times on wide-field microscopes (and not using autoexposure on these systems) can avoid such detrimental mistakes.

* Note that additive color mixing will generate different colors than subtractive mixing of pigment colors where the colors are adsorbed. Computer monitors use additive color mixing (RGB, for red, green, blue) to display color, while color printers use subtractive color mixing to generate colors (typically CMYK, for cyan, magenta, yellow, black). Publishers who print articles with color (including the publisher of this book series) often require images to be submitted in CMYK, not RGB color scheme. Colors may look somewhat different in CMYK format compared to RGB format and should be checked/adjusted before submission. Photoshop, for example, will allow one to interchange the color formats under "Image–Mode" settings.

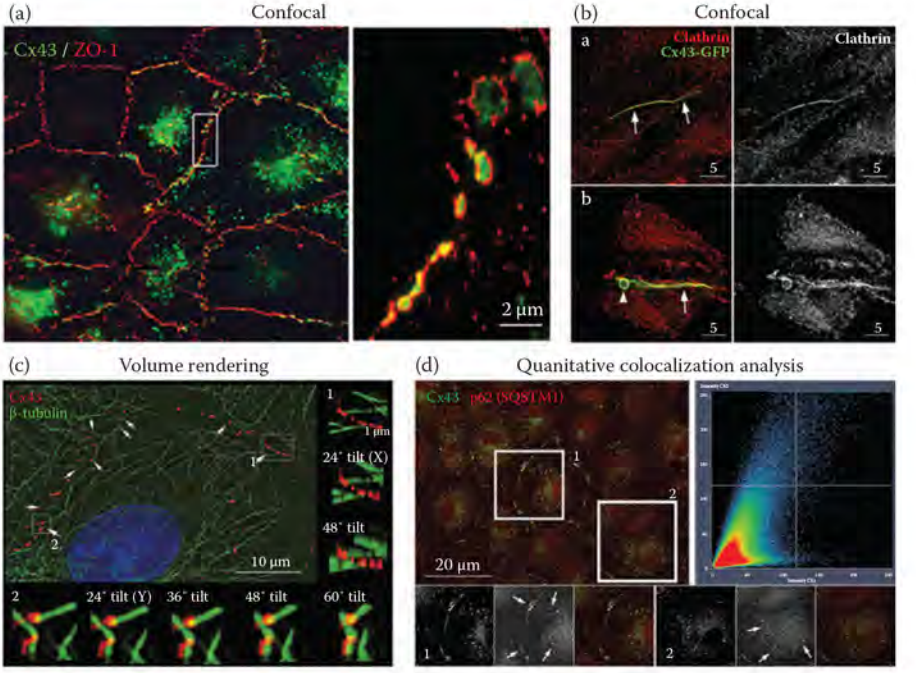

FIGURE 2.12 (See color insert.) Colocalization: Tools and techniques and potential false positives due to emission light bleed-through. (a) Cx43 gap junctions colocalizing with the scaffolding protein, ZO-1, generating a typical rim staining (Hunter et al. 2005), shown in fixed endogenously expressing primary PAECs. (Reprinted from *FEBS Lett*, 582, Baker, S. M., N. Kim, A. M. Gumpert, D. Segretain, and M. M. Falk, Acute internalization of gap junctions in vascular endothelial cells in response to inflammatory mediator-induced G-protein coupled receptor activation, 4039–46, Copyright (2008), with permission from Elsevier.) (b) Gap junctions and AGJs colocalizing with clathrin shown in fixed Cx43-eGFP-expressing HeLa cells. (Reproduced from Piehl, M., C. Lehmann, A. Gumpert, J. P. Denizot, D. Segretain, and M. M. Falk, *Mol Biol Cell*, 18, 337–47, 2007. With permission.) (c) Microtubules attached to Cx43 gap junctions (yellow dots in images of inset 2) shown in fixed and antibody-stained rat 1 cells. (Reprinted from *Curr Biol*, 11, Giepmans, B. N., I. Verlaan, T. Hengeveld, H. Janssen, J. Calafat, M. M. Falk, and W. H. Moolenaar, Gap junction protein connexin-43 interacts directly with microtubules, 1364–8, Copyright (2001), with permission from Elsevier.) To better demonstrate the colocalization, a stack of images in Z was acquired and a volume view was generated and rendered 48° horizontally (inset 1) and 60° sideways (inset 2), respectively. Note that at all angles, attachment points remain and do not spatially separate. (d) The colocalization of the Cx43 and the autophagic protein, p62/sequestosome1/SQSTM1 in PAECs, was demonstrated using an imaging software featuring quantitative colocalization analysis. (Reproduced from Fong, J. T., R. M. Kells, A. M. Gumpert, J. Y. Marzillier, M. W. Davidson, and M. M. Falk, *Autophagy*, 8, 794–811, 2012. With permission.) The fluorescence intensity of each pixel in both channels is analyzed and plotted. The blue signal in the shown scatter plot above the threshold (white lines, in this case, set high) indicates significant colocalization of both proteins.

(*Continued*)

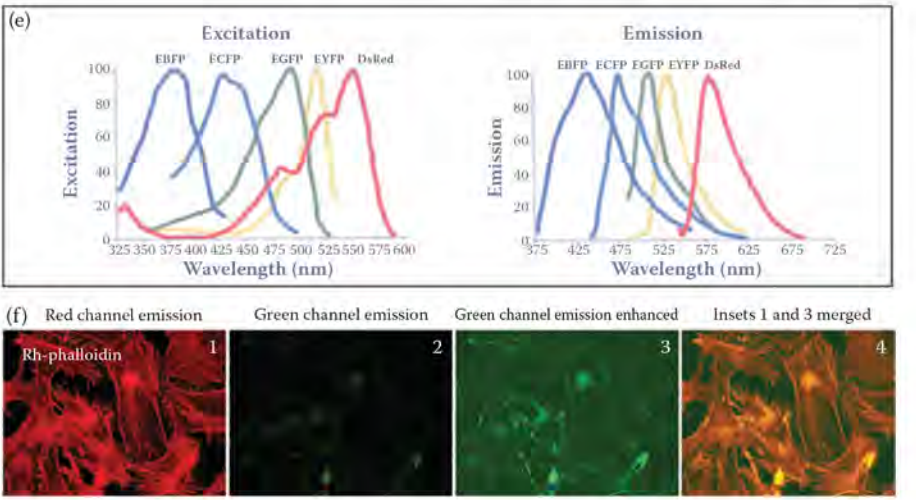

FIGURE 2.12 (CONTINUED) (See color insert.) Colocalization: Tools and techniques and potential false positives due to emission light bleed-through. (e) Excitation and emission spectra of eGFP and color derivatives published by Promega Inc. Note the sometimes substantial overlap in excitation and emission signals requiring adequate excitation and emission bandpass filters, and correct exposure times. (f) A purposely falsified "colocalization" generated by enhancing the green bleed-through signal of the Rhodamine-labeled phalloidin (decorating actin filaments) and merging with the red emission signal to demonstrate that the images used for the colocalization analyses should be acquired at low exposure settings where bleed-through into the other emission channels is not occurring.

As colocalization is often restricted to small areas of the image, it can be more convincing to show additional higher secondary magnification images of selected, cropped areas (as in Figures 2.11d,e, 2.12a,c, and d). Furthermore, as monochrome often shows better than blue, green, or red on black (especially in print), it can be more convincing to show the single-color emission images in black and white and only the merged image in color (compare images in Figure 2.11d and e)*. To collect Z image stacks, reconstructing a volume view and tilting volume views sideways (as shown for microtubules attached to Cx43-based gap junctions in two different areas in Figure 2.12c) can further help to convincingly demonstrate a potential colocalization

* It is advantageous to use CCD cameras that are black and white, not color cameras, as they acquire images at 12- or even 16-bit image depth, compared to only 8 bits of RGB color images (the total bit depth a monitor can display is 24 bits). Also, they are more light sensitive compared to color CCD cameras. Black-and-white CCD cameras provide better images consisting of many more shades of gray (256, 4,096, and 65,536 shades of gray for an 8-, 12-, and 16-bit image, respectively) (Kimpe and Tuytschaever 2007). However, not all applications allow the display of 12- or 16-bit images and need to be converted into 8-bit images, unfortunately with an unavoidable loss of gray scales. This conversion can be done in Photoshop under "Image–Mode" settings. In addition, black-and-white images can be pseudocolored into any color, a feature that is useful to better show the most important object on an image (compare, for example, the images in Figure 2.9f and g in which Cx43-CFP and YFP tubulin are shown in either green or red, respectively) and to visualize the colocalization to red/green color-blind investigators/readers.

(Giepmans et al. 2001). Finally, a quantitative colocalization analysis can make a colocalization analyses even more compelling, especially if the maximum intensity threshold (the intensity of both signals on an image point) is set high. These can be performed with advanced imaging programs that measure the fluorescence intensities of each imaging point and show the values on scatter plots. This was performed with the image shown in Figure 2.12d, where the gap junctions and the AGJs colocalize with the autophagic marker protein, p62 sequestosome1, in endogenously Cx43-expressing primary pulmonary artery epithelial cells (PAECs) (Fong et al. 2012).

2.11 QUANTITATIVE FLUORESCENCE ANALYSES: A FEW EXAMPLES

Fluorescent images and image sequences of gap junctions not only contain a huge amount of qualitative and temporal information but also quantitative data as the fluorescence intensity correlates with the number of fluorophores. For example, quantitative fluorescence intensity analyses over time following photobleaching of the plasma membrane lipid (DiI-labeled) and Cx43-GFP demonstrate that the plasma membrane lipids are highly dynamic, both inside and outside of gap junctions, while the gap junction channels in the gap junction plaques are not. DiI fluorescence photobleached in defined areas inside and outside of gap junctions fully recovers to the prebleach levels within a few seconds, while the Cx43-GFP plaque areas do not (Figure 2.13a through c). These quantitative FRAP analyses were performed on a

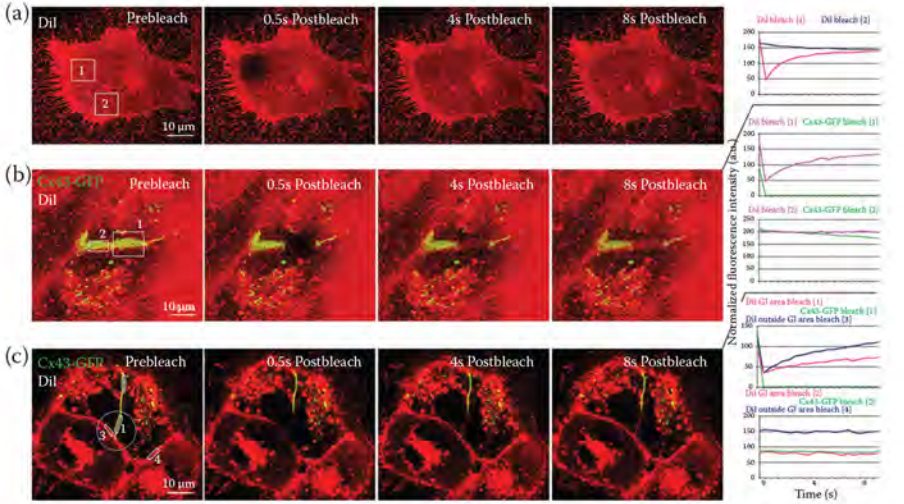

FIGURE 2.13 (See color insert.) Quantitative fluorescence analyses. Fluorescence images not only contain qualitative but also a wealth of quantitative data, as the fluorescence intensity correlates with the number of fluorophores. (a–c) Quantitative fluorescence intensity analyses of time-lapse recordings after permanently photobleaching the lipid (DiI) and the Cx43-GFP gap junction fluorescence in defined areas (boxed areas in (a) and (b) and white-outlined arbitrary areas in (c)). Note the rapid recovery of the lipid fluorescence inside and outside of the gap junctions, while the gap junction dynamics is significantly slower.

(*Continued*)

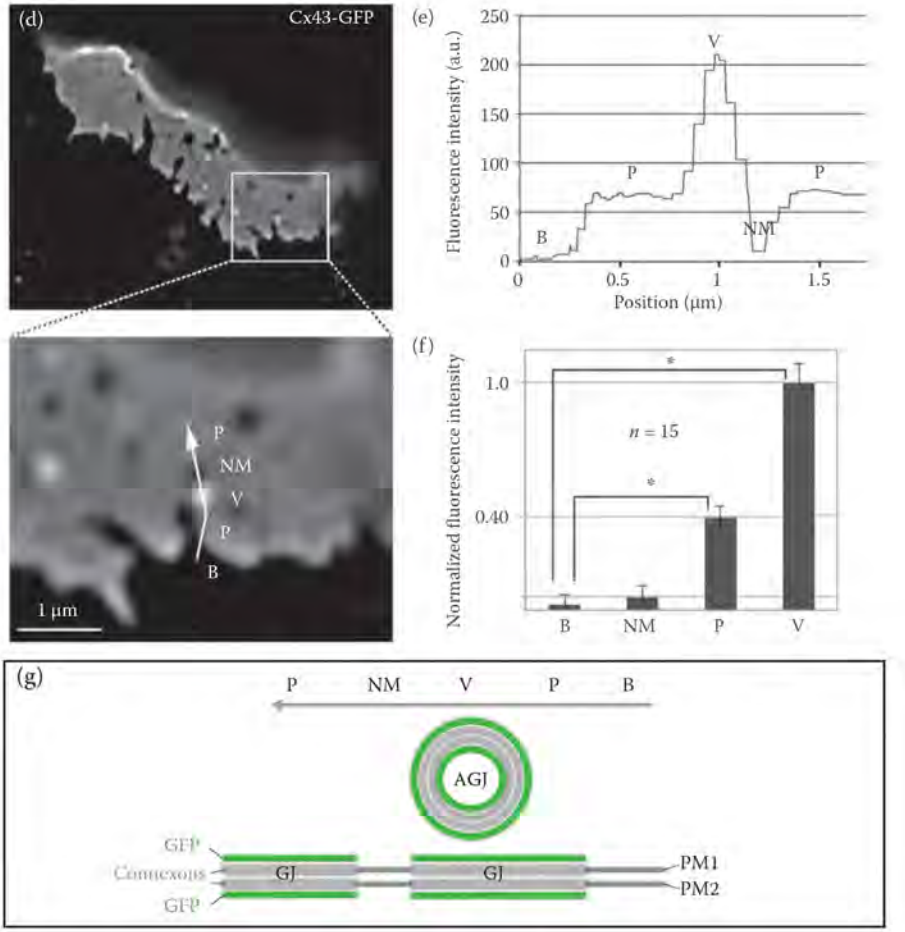

FIGURE 2.13 (CONTINUED) (See color insert.) Quantitative fluorescence analyses. (d–f) Quantitative fluorescence analysis performed along a line shown in the inset in d strategically placed to traverse a portion of a gap junction plaque P, the connexin-free junctional membrane domain inside NM and outside the plaque B, and a vesicle located in front of the plaque V. The fluorescence intensity along the line is shown in (e), and for 15 similar analyses in (f). (G) The schematic representation of the region shown in (d) with the layers of GFP highlighted that correspond to and correlate with the detected fluorescence intensities of areas B, NM, P, and V. (Also see the quantitative fluorescence colocalization analysis shown in Figure 2.12d.) (Reproduced from Falk, M. M., S. M. Baker, A. M. Gumpert, D. Segretain, and R. W. Buckheit III, *Mol Biol Cell*, 20, 3342–52, 2009. With permission.)

Zeiss LSM510 META laser-scanning confocal microscope running software package version 3.0 (Falk et al. 2009). Quantitative FRAP and FLIP experiments shown in Figure 2.10a through f were performed on a BioRad MRC-1024 laser-scanning confocal imaging system.

Furthermore, quantitative fluorescence image analyses also showed that gap junction channels internalized from gap junctions are endocytosed as complete

double-membrane spanning channels and not as connexons (half-channels) (Falk et al. 2009). Figure 2.13d shows a still image of a time-lapse sequence of an en face-viewed gap junction acquired at high primary magnification. Several connexin-free junctional membrane domains within the gap junction (NM, appearing dark), bright fluorescent vesicles (V, AGJs generated by the endocytosis of gap junction plaque portions) in front of the plaque area (P), as well as connexin-free junctional membrane domain surrounding the gap junction plaque (B) are visible (schemed in Figure 2.13g). The fluorescence intensity along a line placed across these regions is shown in Figure 2.13e, and the average of 15 different plaques is shown in Figure 2.13f. Note that regions B and NM have comparable low background fluorescence. The fluorescence intensity in the plaque regions P emitted by two layers of GFP (on both sides of the docked connexons; compare Figure 2.13g) averages about 75 arbitrary fluorescence intensity units. The fluorescence intensity in the region of the AGJ in front of the plaque V is four times higher (averaging about 220 arbitrary units), indicating that four layers of GFP are present in the vesicle (two on the apical side and two on the basal side), totaling six layers of GFP when the vesicle is located in front of the gap junction plaque (as in the example shown in Figure 2.13d,e). These quantitative fluorescence analyses can be quite easily performed with advanced imaging software packages such as NIS Elements (Nikon), MetaVue and MetaMorph (Molecular Devices), Openlab (Improvision), ImageJ (National Institutes of Health, free shareware), etc.

2.12 DATA SIZE

2.12.1 Challenges Related to Acquiring Large Time-Lapse Movie Files

As elaborated earlier, the best means of demonstrating the dynamic movements of gap junctions are time-lapse movie sequences. However, there are a few challenges with time-lapse movies that need to be considered. The raw data generated from time-lapse movies can easily be several hundred megabytes to gigabytes in size depending on the duration of the time lapse, the selection of image intervals, the number of channels acquired, and the number of points selected for study. A large external hard drive of at least several hundred gigabytes to a few terabytes should be available for the long-term storage of the generated data. It is best not to save the time-lapse images on an external drive as the data are generated, because the data transfer speed is often too slow for it to effectively work in real time and may slow down and unintentionally extend the set frame interval. It is better to store the captured frames on the imaging computer's hard drive and only transfer them to the external storage device after acquisition. It is advisable to erase the previous time-lapse movies from the hard drive from time to time, as they will gradually fill up the drive and slow down the computer system if the storage space becomes limited. Of course, a well-planned data filing system is essential if one wants to be able to reliably find and access earlier acquired image data sets.

2.12.2 Compression of Large Image Files for Submission and Publication

For presentation, submission, and publication, movie sequences need to be transferred into compatible formats such as AVI (for personal computers [PCs]), MOV (on Macintosh computers [Macs]), or MPEG which is accepted by Microsoft PowerPoint® and journal publishers. Compatibility issues between MOV and AVI formats unfortunately continue to exist between Macs and PCs, thus downloading a compatible media player that plays all formats (such as VLC or VideoLAN, a free shareware) is advisable. The presentation of movie files and the submission for publication in general also require substantially reducing the file size. Most, if not all, the publishers limit the movie file size to 10 MB. It can be challenging to compress a 100 GB time-lapse recording into such a small size given that some time-lapse recordings may last for many hours. This, for example, was needed for the presentation of the over 20- and 50-hour-long recordings shown in Figure 2.2a and b. We had satisfactory success using QuickTime Pro on a Mac and MPEG movie formats. Finally, as time-lapse movies cannot be published in print, assembling still-image montages consisting of selected frames of the movies that represent the time-lapse events for the physical publication is recommended (see Figures 2.2a,b, 2.7b through f, 2.9f,g, 2.10a through g, 2.11b,c, and 2.13a through c). Publishers in general require that each submitted movie file is represented in the physical manuscript by at least one still image taken from the movie sequence (see the "Instructions to Authors" sections of individual journal/book publishers).

2.13 PRACTICAL CONSIDERATIONS FOR SETTING UP A TIME-LAPSE RECORDING

For routine live-cell recordings of gap junctions, the cells should be passaged 1–2 days beforehand. If the cells stably express the fluorescent connexin (inducible or noninducible expression systems), one only needs to wait for the gap junction plaques to become visible under a conventional fluorescence microscope before beginning a time-lapse experiment. If the cells are transiently transfected, this should be done the day before the imaging for standard observations. Most connexins will form prominent gap junction plaques in cells within 16–24 hours (see Figure 2.8a). Transient transfections can be accomplished using a lipid-based transfection reagent kit such as Superfect (Qiagen) or Lipofectamine 2000 (Invitrogen). Prior to imaging, the culture medium in the dish should be exchanged for fresh medium (not containing phenol red, see Section 2.2.1) to ensure that the cells have a sufficient supply of nutrients for the duration of the experiment. Dead and floating cells should be removed by washes with 1xPBS or culture medium, as these may obscure the imaging of healthy attached cells. Floating cells also often exhibit high autofluorescence, which can disguise the fluorescent signals in the attached cells.

If the cells are to be imaged in glass-bottom dishes, initial condensation tends to build up on the lid of the dish, which requires a few minutes for the conditions to stabilize. Automated image/incubation systems such as the Nikon BioStation will indicate to the user when the temperature in the chamber has equilibrated and stabilized

(approximately 30 minutes). The stabilization period is required to ensure that the system will remain in focus throughout the recording period. Indeed, drifting out of focus is one of the main issues if the temperature in the imaging system is not well equilibrated. Thus, it is generally advisable to begin imaging during the day, periodically review the acquired image sequences, and refocus if necessary before leaving the system to image for extended periods of time, especially overnight. If the live-cell microscope system is equipped with an automatic X/Y stage, it allows the user to select, mark, and revisit multiple points of interest (gap junctions) for the entire duration of the time lapse. In addition, some advanced systems provide an infrared-based focusing system (autofocus) that keeps the distance between the objective lens and the cover glass constant. Of course, if the cells and the gap junctions move in Z, they still may move out of the focal plane.

To avoid the toxic effects resulting from short, high-energy wavelength exposure (e.g., the UV and the blue light used to excite CFP, GFP, etc.), it is advisable to observe the living cells with the lowest possible excitation light intensity and to keep the exposure times to the minimum that will still generate the desired image. The cells may tolerate the exposure to intense light for short times with negligible negative effects; however, in long recordings, the cells will be repeatedly exposed for many hours potentially generating nonphysiological cellular reactions (see Figure 2.2d). To image general gap junction dynamics, acquiring one image every 1–2 minutes while exposing for less than 2 seconds is a good start. In addition to fluorescence images, phase contrast or DIC frame acquisition is advisable, as overlaying the fluorescent and the contrast-enhanced white light images will generate a more comprehensive overview of the imaged cells (as in Figure 2.2a and b). It can also convincingly demonstrate that the suspected gap junction plaque is indeed residing in the lateral plasma membranes (as, e.g., shown in Figures 2.2a,b, 2.3g, 2.6e, 2.9a, and 2.11c).

2.14 CONCLUSIONS

Live-cell imaging of gap junctions is a powerful technique that is especially valuable if carried out together with other ultrastructural, biochemical, and molecular biology analyses. However, it is not a simple and quick technique. It requires dedication, planning, and a passion for microscopy. It is important to select the right imaging system and, as is true for all techniques, it is important to understand the system's abilities and limitations well enough to avoid potentially harmful pitfalls. However, the ability to observe the behavior of connexins and gap junctions in their natural environment, the wealth of acquired qualitative and quantitative spatiotemporal data, and the ability to detect connexins interacting with their various binding partners during their life cycle in real time, in our minds, is clearly worth the investment of time and resources. The continuous development of novel and improved fluorescent probes in combination with the development of enhanced and ever more affordable imaging systems (including superresolution techniques), promises to further increase our ability to investigate gap junctions in living cells in the near future. Finally, as fluorescence imaging is a highly visual technique, convincing data-reach, as well as esthetic images of cells are likely to excite life scientists at all stages of

their careers. It is our hope that the numerous examples, tips, and procedures given in this chapter on how to perform live-cell imaging of connexins and gap junctions will contribute to increasing the excitement.

ACKNOWLEDGMENTS

MMF wishes to thank the many previous and current Falk lab members that over the past two decades have contributed in various successful ways to the live-cell imaging of gap junctions, their dedication, and their constructive criticism. In particular, we thank Dr. Ben N. G. Giepmans for performing the superb recording of an internalizing gap junction shown in Figure 2.11b when visiting my lab as a graduate student and Dr. Lynne Cassimeris, for critically reading and commenting on the paper. Work in the Falk lab is supported by the National Institutes of Health (NIH), National Institute of General Medical Sciences (NIGMS) Grant GM55725 and funds from Lehigh University.

REFERENCES

Baker, S. M., R. W. Buckheit III, and M. M. Falk. 2010. Green-to-red photoconvertible fluorescent proteins: Tracking cell and protein dynamics on standard wide-field mercury arc-based microscopes. *BMC Cell Biol*. no. 11:15.

Baker, S. M., N. Kim, A. M. Gumpert, D. Segretain, and M. M. Falk. 2008. Acute internalization of gap junctions in vascular endothelial cells in response to inflammatory mediator-induced G-protein coupled receptor activation. *FEBS Lett*. no. 582 (29):4039–46.

Bejarano, E., H. Girao, A. Yuste, B. Patel, C. Marques, D. C. Spray, P. Pereira, and A. M. Cuervo. 2012. Autophagy modulates dynamics of connexins at the plasma membrane in a ubiquitin-dependent manner. *Mol Biol Cell*. no. 23 (11):2156–69.

Berthoud, V. M., P. J. Minogue, J. G. Laing, and E. C. Beyer. 2004. Pathways for degradation of connexins and gap junctions. *Cardiovasc Res* no. 62 (2):256–67.

Boassa, D., J. L. Solan, A. Papas, P. Thornton, P. D. Lampe, and G. E. Sosinsky. 2010. Trafficking and recycling of the connexin43 gap junction protein during mitosis. *Traffic*. no. 11 (11):1471–86.

Bukauskas, F. F., K. Jordan, A. Bukauskiene, M. V. Bennett, P. D. Lampe, D. W. Laird, and V. K. Verselis. 2000. Clustering of connexin 43-enhanced green fluorescent protein gap junction channels and functional coupling in living cells. *Proc Natl Acad Sci U S A*. no. 97 (6):2556–61.

Chen, J., L. Pan, Z. Wei, Y. Zhao, and M. Zhang. 2008. Domain-swapped dimerization of ZO-1 PDZ2 generates specific and regulatory connexin43-binding sites. *EMBO J* no. 27 (15):2113–23.

Chudakov, D. M., S. Lukyanov, and K. A. Lukyanov. 2007. Tracking intracellular protein movements using photoswitchable fluorescent proteins PS-CFP2 and Dendra2. *Nat Protoc*. no. 2 (8):2024–32.

Falk, M. M. 2000. Connexin-specific distribution within gap junctions revealed in living cells. *J Cell Sci*. no. 113 (Pt 22):4109–20.

Falk, M. M. 2002. Genetic tags for labelling live cells: Gap junctions and beyond. *Trends Cell Biol*. no. 12 (9):399–404.

Falk, M. M., and N. B. Gilula. 1998. Connexin membrane protein biosynthesis is influenced by polypeptide positioning within the translocon and signal peptidase access. *J Biol Chem*. no. 273 (14):7856–64.

Falk, M. M., and U. Lauf. 2001. High resolution, fluorescence deconvolution microscopy and tagging with the autofluorescent tracers CFP, GFP, and YFP to study the structural composition of gap junctions in living cells. *Microsc Res Tech*. no. 52 (3):251–62.

Falk, M. M., S. M. Baker, A. M. Gumpert, D. Segretain, and R. W. Buckheit III. 2009. Gap junction turnover is achieved by the internalization of small endocytic double-membrane vesicles. *Mol Biol Cell*. no. 20 (14):3342–52.

Falk, M. M., L. K. Buehler, N. M. Kumar, and N. B. Gilula. 1997. Cell-free synthesis and assembly of connexins into functional gap junction membrane channels. *Embo J*. no. 16 (10):2703–16.

Falk, M. M., J. T. Fong, R. M. Kells, M. C. O'Laughlin, T. J. Kowal, and A. F. Thevenin. 2012. Degradation of endocytosed gap junctions by autophagosomal and endo-/lysosomal pathways: A perspective. *J Membr Biol*. no. 245 (8):465–76.

Falk, M. M., R. M. Kells, and V. M. Berthoud. 2014. Degradation of connexins and gap junctions. *FEBS Lett*. no. 588 (8):1221–9.

Falk, M. M., N. M. Kumar, and N. B. Gilula. 1994. Membrane insertion of gap junction connexins: Polytopic channel forming membrane proteins. *J Cell Biol*. no. 127 (2):343–55.

Fong, J. T., R. M. Kells, and M. M. Falk. 2013. Two tyrosine-based sorting signals in the Cx43 C-terminus cooperate to mediate gap junction endocytosis. *Mol Biol Cell*. no. 24 (18):2834–48.

Fong, J. T., R. M. Kells, A. M. Gumpert, J. Y. Marzillier, M. W. Davidson, and M. M. Falk. 2012. Internalized gap junctions are degraded by autophagy. *Autophagy*. no. 8 (5):794–811.

Fort, A. G., J. W. Murray, N. Dandachi, M. W. Davidson, R. Dermietzel, A. W. Wolkoff, and D. C. Spray. 2011. In vitro motility of liver connexin vesicles along microtubules utilizes kinesin motors. *J Biol Chem*. no. 286 (26):22875–85.

Fuller, S. D., R. Bravo, and K. Simons. 1985. An enzymatic assay reveals that proteins destined for the apical or basolateral domains of an epithelial cell line share the same late Golgi compartments. *EMBO J*. no. 4 (2):297–307.

Gaietta, G., T. J. Deerinck, S. R. Adams, J. Bouwer, O. Tour, D. W. Laird, G. E. Sosinsky, R. Y. Tsien, and M. H. Ellisman. 2002. Multicolor and electron microscopic imaging of connexin trafficking. *Science*. no. 296 (5567):503–7.

Giepmans, B. N. G., I. Verlaan, T. Hengeveld, H. Janssen, J. Calafat, M. M. Falk, and W. H. Moolenaar. 2001. Gap junction protein connexin-43 interacts directly with microtubules. *Curr Biol*. no. 11 (17):1364–8.

Griffin, B. A., S. R. Adams, and R. Y. Tsien. 1998. Specific covalent labeling of recombinant protein molecules inside live cells. *Science*. no. 281 (5374):269–72.

Gumpert, A. M., J. S. Varco, S. M. Baker, M. Piehl, and M. M. Falk. 2008. Double-membrane gap junction internalization requires the clathrin-mediated endocytic machinery. *FEBS Letters*. no. 582:2887–92.

Gurskaya, N. G., V. V. Verkhusha, A. S. Shcheglov, D. B. Staroverov, T. V. Chepurnykh, A. F. Fradkov, S. Lukyanov, and K. A. Lukyanov. 2006. Engineering of a monomeric green-to-red photoactivatable fluorescent protein induced by blue light. *Nat Biotechnol*. no. 24 (4):461–5.

Hesketh, G. G., M. H. Shah, V. L. Halperin, C. A. Cooke, F. G. Akar, T. E. Yen, D. A. Kass, C. E. Machamer, J. E. Van Eyk, and G. F. Tomaselli. 2010. Ultrastructure and regulation of lateralized connexin43 in the failing heart. *Circ Res*. no. 106 (6):1153–63.

Hunter, A. W., R. J. Barker, C. Zhu, and R. G. Gourdie. 2005. Zonula occludens-1 alters connexin43 gap junction size and organization by influencing channel accretion. *Mol Biol Cell*. no. 16 (12):5686–98.

Ivanov, A. I., I. C. McCall, C. A. Parkos, and A. Nusrat. 2004a. Role for actin filament turnover and a myosin II motor in cytoskeleton-driven disassembly of the epithelial apical junctional complex. *Mol Biol Cell*. no. 15 (6):2639–51.

Ivanov, A. I., A. Nusrat, and C. A. Parkos. 2004b. Endocytosis of epithelial apical junctional proteins by a clathrin-mediated pathway into a unique storage compartment. *Mol Biol Cell*. no. 15 (1):176–88.

Johnson, K. E., S. Mitra, P. Katoch, L. S. Kelsey, K. R. Johnson, and P. P. Mehta. 2013. Phosphorylation on serines 279 and 282 of connexin43 regulates endocytosis and gap junction assembly in pancreatic cancer cells. *Mol Biol Cell*. no. 24:715–33.

Jordan, K., J. L. Solan, M. Dominguez, M. Sia, A. Hand, P. D. Lampe, and D. W. Laird. 1999. Trafficking, assembly, and function of a connexin43-green fluorescent protein chimera in live mammalian cells. *Mol Biol Cell*. no. 10 (6):2033–50.

Kalmatsky, B. D., Y. Batir, T. A. Bargiello, and T. L. Dowd. 2012. Structural studies of N-terminal mutants of connexin 32 using (1)H NMR spectroscopy. *Arch Biochem Biophys*. no. 526:1–8.

Kalmatsky, B. D., S. Bhagan, Q. Tang, T. A. Bargiello, and T. L. Dowd. 2009. Structural studies of the N-terminus of connexin 32 using 1H NMR spectroscopy. *Arch Biochem Biophys*. no. 490 (1):9–16.

Kelly, S. M., J. K. Vanslyke, and L. S. Musil. 2007. Regulation of ubiquitin-proteasome system mediated degradation by cytosolic stress. *Mol Biol Cell*. no. 18 (11):4279–91.

Kimpe, T., and T. Tuytschaever. 2007. Increasing the number of gray shades in medical display systems—How much is enough? *J Digit Imaging*. no. 20 (4):422–32.

Koval, M. 2006. Pathways and control of connexin oligomerization. *Trends Cell Biol*. no. 16 (3):159–66.

Laing, J. G., and E. C. Beyer. 1995. The gap junction protein connexin43 is degraded via the ubiquitin proteasome pathway. *J Biol Chem*. no. 270 (44):26399–403.

Laing, J. G., P. N. Tadros, E. M. Westphale, and E. C. Beyer. 1997. Degradation of connexin43 gap junctions involves both the proteasome and the lysosome. *Exp Cell Res*. no. 236 (2):482–92.

Laird, D. W. 1996. The life cycle of a connexin: Gap junction formation, removal, and degradation. *J Bioenerg Biomembr*. no. 28 (4):311–8.

Laird, D. W., K. Jordan, T. Thomas, H. Qin, P. Fistouris, and Q. Shao. 2001. Comparative analysis and application of fluorescent protein-tagged connexins. *Microsc Res Tech*. no. 52 (3):263–72.

Lauf, U., P. Lopez, and M. M. Falk. 2001. Expression of fluorescently tagged connexins: A novel approach to rescue function of oligomeric DsRed-tagged proteins. *FEBS Lett*. no. 498 (1):11–5.

Lauf, U., B. N. Giepmans, P. Lopez, S. Braconnot, S. C. Chen, and M. M. Falk. 2002. Dynamic trafficking and delivery of connexons to the plasma membrane and accretion to gap junctions in living cells. *Proc Natl Acad Sci U S A*. no. 99 (16):10446–51.

Leithe, E., A. Kjenseth, S. Sirnes, H. Stenmark, A. Brech, and E. Rivedal. 2009. Ubiquitylation of the gap junction protein connexin-43 signals its trafficking from early endosomes to lysosomes in a process mediated by Hrs and Tsg101. *J Cell Sci*. no. 122 (Pt 21):3883–93.

Lichtenstein, A., P. J. Minogue, E. C. Beyer, and V. M. Berthoud. 2011. Autophagy: A pathway that contributes to connexin degradation. *J Cell Sci*. no. 124 (Pt 6):910–20.

Lippincott-Schwartz, J., and G. H. Patterson. 2009. Photoactivatable fluorescent proteins for diffraction-limited and super-resolution imaging. *Trends Cell Biol*. no. 19 (11):555–65.

Lopez, P., D. Balicki, L. K. Buehler, M. M. Falk, and S. C. Chen. 2001. Distribution and dynamics of gap junction channels revealed in living cells. *Cell Commun Adhes*. no. 8 (4–6):237–42.

Los, G. V., L. P. Encell, M. G. McDougall, D. D. Hartzell, N. Karassina, C. Zimprich, M. G. Wood et al. 2008. HaloTag: A novel protein labeling technology for cell imaging and protein analysis. *ACS Chem Biol*. no. 3 (6):373–82.

Maeda, S., S. Nakagawa, M. Suga, E. Yamashita, A. Oshima, Y. Fujiyoshi, and T. Tsukihara. 2009. Structure of the connexin 26 gap junction channel at 3.5 A resolution. *Nature*. no. 458 (7238):597–602.

Matlin, K. S., and K. Simons. 1983. Reduced temperature prevents transfer of a membrane glycoprotein to the cell surface but does not prevent terminal glycosylation. *Cell*. no. 34 (1):233–43.

Musil, L. S., and D. A. Goodenough. 1993. Multisubunit assembly of an integral plasma membrane channel protein, gap junction connexin43, occurs after exit from the ER. *Cell*. no. 74 (6):1065–77.

Nickel, B. M., B. H. DeFranco, V. L. Gay, and S. A. Murray. 2008. Clathrin and Cx43 gap junction plaque endoexocytosis. *Biochem Biophys Res Commun*. no. 374 (4):679–82.

Nimlamool, W., R. M. Kells Andrews, and M. M. Falk. 2015. Connexin43 phosphorylation by PKC and MAPK signals VEGF-mediated gap junction internalization. *Mol Biol Cell*. no. 26 (15):2755–68.

Piehl, M., C. Lehmann, A. Gumpert, J. P. Denizot, D. Segretain, and M. M. Falk. 2007. Internalization of large double-membrane intercellular vesicles by a clathrin-dependent endocytic process. *Mol Biol Cell*. no. 18 (2):337–47.

Purnick, P. E., D. C. Benjamin, V. K. Verselis, T. A. Bargiello, and T. L. Dowd. 2000. Structure of the amino terminus of a gap junction protein. *Arch Biochem Biophys*. no. 381 (2):181–90.

Qin, H., Q. Shao, S. A. Igdoura, M. A. Alaoui-Jamali, and D. W. Laird. 2003. Lysosomal and proteasomal degradation play distinct roles in the life cycle of Cx43 in gap junctional intercellular communication-deficient and competent breast tumor cells. *J Biol Chem*. no. 278 (32):30005–14.

Rhett, J. M., and R. G. Gourdie. 2012. The perinexus: A new feature of Cx43 gap junction organization. *Heart Rhythm*. no. 9 (4):19–23.

Rotundo, R. L., and D. M. Fambrough. 1980. Secretion of acetylcholinesterase: Relation to acetylcholine receptor metabolism. *Cell*. no. 22 (2 Pt 2):595–602.

Saraste, J., and E. Kuismanen. 1984. Pre- and post-Golgi vacuoles operate in the transport of Semliki Forest virus membrane glycoproteins to the cell surface. *Cell*. no. 38 (2):535–49.

Saraste, J., G. E. Palade, and M. G. Farquhar. 1986. Temperature-sensitive steps in the transport of secretory proteins through the Golgi complex in exocrine pancreatic cells. *Proc Natl Acad Sci U S A*. no. 83 (17):6425–9.

Schlingmann, B., P. Schadzek, F. Hemmerling, F. Schaarschmidt, A. Heisterkamp, and A. Ngezahayo. 2013. The role of the C-terminus in functional expression and internalization of rat connexin46 (rCx46). *J Bioenerg Biomembr*. no. 45 (1–2):59–70.

Schmoranzer, J., M. Goulian, D. Axelrod, and S. M. Simon. 2000. Imaging constitutive exocytosis with total internal reflection fluorescence microscopy. *J Cell Biol*. no. 149 (1):23–32.

Shaner, N. C., R. E. Campbell, P. A. Steinbach, B. N. Giepmans, A. E. Palmer, and R. Y. Tsien. 2004. Improved monomeric red, orange and yellow fluorescent proteins derived from Discosoma sp. red fluorescent protein. *Nat Biotechnol*. no. 22 (12):1567–72.

Shaner, N. C., G. H. Patterson, and M. W. Davidson. 2007. Advances in fluorescent protein technology. *J Cell Sci*. no. 120 (Pt 24):4247–60.

Shaw, R. M., A. J. Fay, M. A. Puthenveedu, M. von Zastrow, Y. N. Jan, and L. Y. Jan. 2007. Microtubule plus-end-tracking proteins target gap junctions directly from the cell interior to adherens junctions. *Cell*. no. 128 (3):547–60.

Shcherbakova, D. M., P. Sengupta, J. Lippincott-Schwartz, and V. V. Verkhusha. 2014. Photocontrollable fluorescent proteins for superresolution imaging. *Annu Rev Biophys*. no. 43:303–29.

Stout, R. F. Jr., E. L. Snapp, and D. C. Spray. 2015. Connexin type and fluorescent protein fusion tag determine structural stability of gap junction plaques. *J. Biol. Chem*. no. 290 (39):23497–514.

Thévenin, A. F., T. J. Kowal, J. T. Fong, R. M. Kells, C. G. Fisher, and M. M. Falk. 2013. Proteins and mechanisms regulating gap junction assembly, internalization and degradation. *Physiology*. no. 28 (4):93–116.

Thomas, T., K. Jordan, J. Simek, Q. Shao, C. Jedeszko, P. Walton, and D. W. Laird. 2005. Mechanisms of Cx43 and Cx26 transport to the plasma membrane and gap junction regeneration. *J Cell Sci*. no. 118 (Pt 19):4451–62.

Toomre, D., J. A. Steyer, P. Keller, W. Almers, and K. Simons. 2000. Fusion of constitutive membrane traffic with the cell surface observed by evanescent wave microscopy. *J Cell Biol*. no. 149 (1):33–40.

Wang, H. Y., Y. P. Lin, C. K. Mitchell, S. Ram, and J. O'Brien. 2015. Two-color fluorescent analysis of connexin 36 turnover: Relationship to functional plasticity. *J Cell Sci*. no. 128 (21):3888–97.

Xiao, D., S. Chen, Q. Shao, J. Chen, K. Bijian, D. W. Laird, and M. A. Alaoui-Jamali. 2014. Dynamin 2 interacts with connexin 26 to regulate its degradation and function in gap junction formation. *Int J Biochem Cell Biol*. no. 55:288–97.